SINGLE CELL SEQUENCING OF RADIAL GLIA PROGENY REVEALS DIVERSITY OF NEWBORN NEURONS IN THE ADULT ZEBRAFISH BRAIN

Christian Lange[1], Fabian Rost[2,3], Anja Machate[1], Susanne Reinhardt[1,4], Matthias Lesche[1,4], Anke Weber[1], Veronika Kuscha[1], Andreas Dahl[1,4], Steffen Rulands[2,3] and Michael Brand[1*]*

[1] Center for Regenerative Therapies Dresden (CRTD), CMCB, Technische Universität Dresden, Fetscherstr. 105, 01307, Dresden, Germany.

[2] Max Planck Institute for the Physics of Complex Systems, Noethnitzer Str. 38, 01187 Dresden, Germany

[3] Center for Systems Biology Dresden (CSBD), Pfotenhauer Str. 108, 01307 Dresden, Germany.

[4] DRESDEN-*concept* Genome Center, c/o Center for Molecular and Cellular Bioengineering (CMCB), Technische Universität Dresden, Fetscherstr. 105, 01307, Dresden, Germany

[*] corresponding author

Correspondence: michael.brand@tu-dresden.de and christian.lange3@tu-dresden.de

KEYWORDS:

adult neurogenesis, zebrafish, radial glia, neural stem cell, telencephalon, single cell sequencing

SUMMMARY STATEMENT:

A combination of lineage tracing and single cell sequencing identifies specific markers and functional subpopulations of adult newborn neurons in the zebrafish forebrain.

ABSTRACT

Zebrafish display widespread and pronounced adult neurogenesis, which is fundamental for their regeneration capability after central nervous system injury. However, the cellular identity and the biological properties of adult newborn neurons are elusive for most brain areas.

Here, we used short-term lineage tracing of radial glia progeny to prospectively isolate newborn neurons from the her4.1^{+} radial glia lineage in the homeostatic adult forebrain. Transcriptome analysis of radial glia, newborn neurons and mature neurons using single cell sequencing identified distinct transcriptional profiles including novel markers for each population. Specifically, we detected 2 separate newborn neuron types, which showed diversity of cell fate commitment and location. Further analyses showed homology of these cell types to neurogenic cells in the mammalian brain, identified neurogenic commitment in proliferating radial glia and indicated that glutamatergic projection neurons are generated in the adult zebrafish telencephalon.

Thus, we prospectively isolated adult newborn neurons from the adult zebrafish forebrain, identified markers for newborn and mature neurons in the adult brain, revealed intrinsic heterogeneity among adult newborn neurons and their homology to mammalian adult neurogenic cell types.

INTRODUCTION

Adult neurogenesis, the generation and integration of additional neurons to the brain circuitry in adulthood is widespread across vertebrates, though the extent greatly varies among species (Kaslin et al., 2008; Grandel and Brand, 2013; Alunni and Bally-Cuif, 2016;). It is implicated to support learning and memory (Aimone et al., 2014; Frisen, 2016), but can also function to replace neurons that are lost due to disease or injury in some species (Reimer et al., 2008; Berg et al., 2010; Kroehne et al., 2011; März et al., 2011; Baumgart et al., 2012; Amamoto et al., 2016; Kaslin et al., 2017)

In most mammals, adult neurogenesis is confined to the major neurogenic niches in the subgranular zone of the hippocampal dentate gyrus and the sub-ependymal zone of the lateral ventricles. Newborn neurons (NBNs) integrate only into the granular zone of the dentate gyrus, and the olfactory bulb in rodents or the striatum in humans, respectively (Aimone et al., 2014; Ernst and Frisen, 2015). Outside of these target zones for adult neurogenesis, integration of NBNs is essentially absent or minimal, and most brain areas (including the cerebral cortex) show limited potential for NBN integration and survival, even after injury-induced neuronal cell death (Bhardwaj et al., 2006; Ohab et al., 2006; Saha et al., 2013; Huttner et al., 2014). Thus, a low potential for NBN integration in most brain areas represents an important roadblock for brain repair after injury or neurodegeneration. To develop therapeutic strategies for cell replacement, a better understanding of the mechanisms that might allow neurogenesis and neuron integration in such brain areas is needed.

In contrast to mammals, teleost fish display widespread and pronounced adult neurogenesis (Ekstrom et al., 2001; Zupanc et al., 2005; Adolf et al., 2006; Grandel et al., 2006; Alunni et al., 2010; Ganz and Brand, 2015). In the adult zebrafish brain, we previously identified 17 different proliferative zones throughout the neuraxis. These

proliferative zones are accompanied by adjacent zones, where newborn neurons integrate. In the telencephalon, the cell bodies of radial glia (RG) neural stem cells are localized in the ventricular zone (VZ), but they span the entire telencephalon with their processes (Grandel et al., 2006; Adolf et al., 2006; Ganz et al., 2010). In the dorsal telencephalon (pallium), RG divide constitutively in adulthood and give rise to neurons, which undergo short-distance migration to the adjacent peri-ventricular zone (PVZ) of the parenchyma, where they are added to the circuitry (Ganz et al., 2010; Kroehne et al., 2011; Furlan et al., 2017). Cells in the PVZ express markers of glutamatergic projection neuron development, such as *tbr1, neurod1 and bhlhe22* (Ganz et al., 2012; Furlan et al., 2017). Similar to the developing mammalian forebrain, a second population of neural progenitors, expressing the marker nestin, exists in the VZ of the striatal ventral telencephalon, which expresses markers of GABAergic interneuron progenitors, e.g. *dlx2* and *dlx5a* (März et al., 2010a; Ganz et al., 2012). The ventrally generated neurons undergo long-distance migration into the telencephalic parenchyma, reminiscent of interneuron tangential migration in mammalian development (Ganz et al., 2010). These data indicate that in zebrafish telencephalon, the dorsal pallium and the ventral striatum –corresponding to the cognate mammalian brain territories – display ongoing neurogenesis and NBN integration in an evolutionarily conserved manner.

In contrast to mammals, zebrafish efficiently repair lesions after injury to the telencephalon through induction of i) proliferation of radial glia, ii) neuron generation and iii) integration of newborn, differentiated neurons in the parenchyma (Kroehne et al., 2009; Kroehne et al., 2011; Baumgart et al., 2012; März et al., 2011; Skaggs et al., 2014). Within weeks and months after the injury, the lesion site is dramatically reduced in size and neuronal connections in the lesioned hemisphere, which are initially destroyed, re-appear. Lineage tracing shows that these regenerated neurons derive

from RG and persist long-term (Kroehne et al., 2011). The molecular mechanisms that enable this repair process are currently incompletely understood. In particular, previous research focused on the regulation of RG as the source of NBNs in homeostasis or after injury, while the role of immature, neuronally committed progenitor cells and neurons, at various stages of their maturation and integration into the adult telencephalon remains poorly understood.

Recently, cellular differentiation trajectories were reconstructed using single cell sequencing – alone or in combination with cellular barcoding – in vertebrate embryos (Alemany et al., 2018; Briggs et al., 2018; Farrell et al., 2018; Spanjaard et al., 2018; Wagner et al., 2018) or in the zebrafish juvenile brain (Raj et al., 2018). However, neurogenesis and NBN differentiation in the adult telencephalon has not been investigated using these methods. To gain insight into the role and regulation of NBNs in adult neurogenesis in the zebrafish forebrain, we devised a strategy to lineage trace RG, RG-derived NBNs and MNs, allowing their direct, specific isolation from heterogenous cell populations (i.e. prospective isolation). Transcriptome analysis by single-cell sequencing revealed pronounced heterogeneity among RG-derived NBNs and allowed to analyze the differentiation trajectories in the adult zebrafish forebrain.

RESULTS

LINEAGE TRACING OF RADIAL GLIA-DERIVED NEWBORN NEURONS IN THE ADULT ZEBRAFISH TELENCEPHALON.

In order to prospectively isolate the neuronal progeny of radial glia (i. e. NBNs) in the adult zebrafish telencephalon, we developed a short-term lineage-tracing protocol, based on retention of fluorescent proteins in cell-type-specific, fluorescent reporter lines. To this end, we combined the neuronal reporter line *elavl3:gfp* (Park et al., 2000) with the *her4.1:mcherry* reporter line that marks RG (Kroehne et al., 2011). Although

the expression of *mcherry* mRNA under the control of the her4.1 promotor is restricted to radial glia and rapidly downregulated in NBN, fluorescent proteins, which have a half-life of circa 24 hours (Li et al., 1998), are inherited by the neuronal daughters of dividing radial glia in detectable amounts (Furlan et al., 2017). Using this approach, newborn neurons could be identified as mcherry/GFP double-positive cells in the telencephalon of *her4.1:mcherry*; *elavl3:gfp* fish (Fig. 1A). When analyzing dissociated cells from *her4.1:mcherry*; *elavl3:gfp* forebrains, consisting of the telencephalon and anterior diencephalon (see Fig. 1B and materials and methods) with flow cytometry, we found that cells with high levels of mcherry were GFP-negative. In contrast, cells with low, but detectable levels of mcherry were clearly positive for the neuronal marker *elavl3*:GFP (Fig. 1C). These results confirmed our hypothesis that NBNs can be identified as mcherry/GFP double-positive cells in the telencephalon of *her4.1:mcherry*;*elavl3:gfp* fish, while *bona fide* RG had higher average levels of mcherry, but were GFP-negative. Forebrain cells from single-transgenic *her4.1:mcherry* or *elavl3:gfp* fish contained only few mcherry and GFP double positive cells, which are likely autofluorescent cells (Fig. S1A). Quantification showed that mcherry^{high}/GFP^{neg} RG represented 8.7%, while mcherry^{low}/GFP^{pos} cells (designated as NBNs) accounted for 10.9% of all live forebrain cells. Mature neurons (MN; mcherry^{neg}/GFP^{pos}) were the dominating cell population in the adult forebrain with 72.1%, and lineage marker negative cells accounted for 8.2% of forebrain cells (Fig. 1D). Direct imaging of dissociated cells by Image Stream flow cytometry confirmed the presence of single cells that are simultaneously positive for mcherry and GFP, excluding the alternative possibility that these cells might have represented doublets of cells expressing either GFP or mcherry (Fig. 1E).

Since her4.1 is a main target gene of the Notch pathway, mcherry^{low}/GFP^{pos} cells could also represent mature neurons with low level activation of this pathway instead of being NBNs that inherited mcherry protein from their RG precursors. To exclude this possibility, we combined the *elavl3:gfp* neuronal reporter line with a newly generated radial glia specific reporter line: *gfap:nls-cherry*, which expresses nuclear-localized mcherry in telencephalic radial glia cells (Fig. S1B) under the control of the radial glia-specific *gfap* promotor (Bernardos and Raymond, 2006). Flow cytometry of dissociated forebrain cells from *gfap:nls-cherry*; *elavl3:gfp* fish also identified a specific population of mcherry^{low}/GFP^{pos} neurons (Fig. S1C,D). Quantification confirms similar percentages of mcherry^{high}/GFP^{neg} and mcherry^{low}/GFP^{pos} cells (Fig. S1E). To verify that the mcherry^{low}/GFP^{pos} double-positive population is enriched with adult generated neurons, an EdU pulse-chase analysis was performed. Adult *her4.1:mcherry*; *elavl3*:*gfp* fish were injected 3 times with EdU in 12 hour intervals to label sufficient numbers of proliferating cells in the adult brain. EdU incorporation was assessed at 2 hours, 7 days or 4 weeks after the last injection to identify proliferating cells and their immediate progeny, early progeny and late progeny of the initially proliferating cells, respectively (Fig. 2A). After 2 hours of chase, mcherry^{high}/GFP^{neg} RG were the most intensively proliferating cell type as 7.8±2.1% of all cells were EdU^{pos}, while only 0.8±0.3% of mcherry^{low}/GFP^{pos} cells and 0.1±0.01% of mcherry^{neg}/GFP^{pos} mature neurons were EdU^{pos} (Fig 2B,C). In contrast, after 7 hours of EdU chase, EdU incorporation in mcherry^{low}/GFP^{pos} neurons was significantly increased to 11.6±2.1%, while it remained similar in mcherry^{high}/GFP^{neg} RG (10.6±3.5%) and mcherry^{neg}/GFP^{pos} neurons (1.5±0.8%). After 4 weeks of chase, EdU incorporation in mcherry^{low}/GFP^{pos} neurons was reduced to 0.7±0.1% compared with the 7 days chase, mcherry^{high}/GFP^{neg} RG showed a trend towards reduced EdU incorporation (3.9±1.6%), while mcherry^{neg}/GFP^{pos} neurons showed no significant change

(0.6±0.1%)(Fig 2B,C). These data indicate that mcherry^{low}/GFP^{pos} neurons are specifically enriched for adult-generated neurons and suggest that these cells represent a transient population that retains *her4.1*:mcherry at least for 7 days but not anymore at 4 weeks after their generation from mcherry^{high}/GFP^{neg} RG.

Together, these data provide substantial evidence that radial glia-derived NBNs in the adult zebrafish forebrain can be identified by retention of fluorescent proteins expressed in radial glia with simultaneous expression of a neuronal marker. Our analyses reveal a population of NBNs that is equal in number compared to the *her4.1*:mcherry^{high}/*elavl3*:GFP^{neg} bona fide RG.

SINGLE CELL SEQUENCING IDENTIFIES TRANSCRIPTOME PROFILES OF RADIAL GLIA, NEWBORN NEURONS AND MATURE NEURONS IN THE ADULT ZEBRAFISH TELENCEPHALON.

Next, using our lineage tracing protocol, we sorted 171 RG (mcherry^{high}/GFP^{neg}), 169 NBNs (mcherry^{low}/GFP^{pos}) and 30 mature neurons (MNs, mcherry^{neg}/GFP^{pos}) from the adult telencephalon of 6 fish and sequenced them using SMARTSeq2 (Picelli et al., 2014). On average, we detected 1408 expressed genes and 191k transcripts per cell. 264 cells (71%) passed our quality control. This led to 76, 162 and 26 cells from the RG, NBN and MN FACS gates, respectively that were used for downstream analysis. Consistent with our lineage tracing paradigm, cells sorted as RG, but not those sorted as neurons, expressed radial glia markers (*her4.1*, *cx43*, *id1*, *s100b*) (Grandel et al., 2006; Adolf et al., 2006; Kunze et al., 2009; Ganz et al., 2010; Rodriguez Viales et al., 2015) (Fig. 3A). Cells sorted as NBNs expressed pan-neuronal markers and early neuronal markers (*elavl3*, *map2*, *insm1a*) (Ferri and Levitt, 1993; Park et al., 2000; Raj et al., 2018), but showed minimal expression of mature synaptic proteins such as synaptic vesicle protein 2a (*sv2a*), neurogranin a (*nrgna)* and calmodulin-dependent kinase 2a (*camk2a*) (Zhong and

Gerges, 2012), compared to mature neurons (Fig. 3A). We used Louvain clustering to identify 5 clusters with distinct transcriptomic profiles which we visualized by t-stochastic neighbor embedding (t-SNE) as well as principal component analysis (Fig. 3B,C; Fig. S2A,B). The cells from the 3 FACS gates segregated into 5 transcriptome clusters: One cluster (RG) consisted almost exclusively of cells sorted as RG, three clusters (NBN.1, NBN.2 and OPC) contained mostly cells sorted as NBN, and one mixed cluster (MN) contained cells from the NBN and MN gates (Fig. 3B, Fig. S2A). We assigned cell type identity to each cluster based on known marker genes (Fig. 3B): The radial glia marker *her4.1* was expressed specifically in the RG cluster, but not in the neuronal clusters NBN.1, NBN.2 and MN, which all expressed *elavl3*. *sv2a* was sparsely expressed in NBN.1 and NBN.2, but strongly enriched in cluster MN, confirming that MN contained mature neurons. Cells of the OPC cluster also expressed *elavl3* and were identified as oligodendrocyte progenitor cells by the expression of *olig2* (Park et al., 2007)(Fig. 3B,C). The transcriptome analyses identified several marker genes for each of the identified clusters, which allowed their biological characterization (Fig. 2C, Table1). The RG cluster expressed several known RG markers, e.g. *fabp7a* (also known as blbp), *her4.1* and *glula* (encoding glutamine synthase), but also novel markers such as *si:ch211-251b21.1* (encoding the glutamate receptor grik-1), *si:ch211-2111b21.1 (encoding* fgfbp3*)*, *atp1a1b*, *sepp1a*, and *mdka*. The major pure NBN cluster (NBN.1) was characterized by specific expression of *tubb5*, *cd99l2*, *ppp1r14ba*, *cnp* and *tubb2b*. The smaller pure NBN cluster (NBN.2) expressed the transcription factor *ebf3a*, *si:dkey106c17.3* (encoding kcnj19a), *tbr1b*, *msi2b* and *podxl2*. The mixed NBN and MN cluster (cluster MN) showed specific expression of *sult4a1*, *sybu, ube2ka*, *gad1b*, and *sprn2*, while the OPC cluster predominantly expressed the marker genes *aplnra*, *sema5a, si:ch211-286c4.6* (encoding cd59)***,*** ***traf4,*** *cd82a*, which were recently identified as genes expressed in

zebrafish OPCs (Kroehne et al., 2017; Raj et al., 2018). Together, these data show that radial glia-derived NBNs are a heterogeneous population, comprising at least 3 populations (NBN.1, NBN.2 and a part of the MN cluster) with distinct transcriptional profiles. They are distinct from their radial glia precursors, but a subset of NBNs clusters together with mature, synaptically integrated neurons, suggesting that this population represents a more mature state of adult-generated neurons. Interestingly, one minor cluster, comprised of NBNs, none of which expressed *her4.1*, but did express *elavl3,* was identified as oligodendrocyte precursors due to expression of cell-type specific markers (Figs. 3B,C; S4A). Retention of *mcherry*, expressed from a RG-specific promotor in these OPCs, as well as shared marker expression (e.g. *fabp7a*, *slc1a2b*, *atp1a1b*, *cd82a*, *cxcl12a, glula*; see Fig. 3C) supports their generation from RG in the adult zebrafish brain. In addition, flow cytometry of double transgenic fish that combine the RG-specific *her4.1*:mcherry reporter with the OPC-specific reporter *olig2*:*gfp* (Shin et al. 2003; Kroehne et al. 2017; Tsata et al. 2019) (Tg(*her4.1:mcherry*; *olig2:gfp*)) revealed that 28.6±3.9% of all *olig2*:GFP cells were mcherry^{low}/GFP^{high} double-positive (Fig. S4B,C). We also observed numerous cells showing high levels of mcherry fluorescence and low levels of *olig2*-driven GFP fluorescence, possibly representing nascent RG progeny differentiating towards OPCs (Fig. S4B). In summary, these data provide robust evidence that *her4.1*-expressing RG generate heterogeneous and diverse progeny comprising different neuronal and oligodendroglial cell types in the normal adult telencephalon.

ANALYSIS OF GENE EXPRESSION TRAJECTORIES REVEALS DICHOTOMIC DIFFERENTIATION PATTERNS OF RG PROGENY.

To infer the differentiation trajectories of radial glia-derived NBNs, we performed pseudotime-based ordering of our single cell gene expression profiles based on diffusion maps (Fig. 4A). In contrast to dimensionality reduction by t-SNE, diffusion maps retain the global structure of the transcriptomes, such that continuous branching lineages can be visualized (Haghverdi et al., 2015). Using RGs as a root group, pseudotemporal ordering using the diffusion pseudotime algorithm revealed the NBN.1 cluster as the differentiation state that is closely related to RGs. From the NBN.1 cluster, a trajectory branchpoint was formed, leading to the MN cluster or the NBN.2 cluster, respectively. Among these two endpoints, the NBN.2 cluster was the most distant from RGs (Fig. 4A). The OPC cluster was omitted from this analysis for clarity because it was transcriptionally disconnected from the other cells (Fig. S5A).

Next, we compared the different cell clusters to neurogenic cell types in the adult mammalian brain. A recent study generated sc-transcriptome profiles of radial glia, radial glia-like neural stem cells, their neuronal progeny and niche cells in the adult hippocampus and during hippocampal development (Hochgerner et al., 2018). For a combined cell type homology analysis, we transformed the transcriptomes of zebrafish and mouse cells into a transcriptome of all orthologues gene pairs (see Materials and Methods). Then, we performed hierarchical clustering of the zebrafish and murine cell types (Fig. 4B). The zebrafish cell clusters clustered together with different murine neuronal and glial cell types, indicating a dominance of cell type differences of the transcriptional profiles over species differences. In line with our assignment of cell identity, RG clustered together with murine ependymal cells and young astrocytes and zebrafish OPCs clustered with murine OPCs and oligodendrocytes. Interestingly,

NBN.1 cells formed a cluster with murine immature granule cells and pyramidal neurons, while NBN.2 and MN cells clustered together with mature neurons (Fig. 4B). All cell types showed a comparable distribution of similarity of zebrafish cells to their most similar murine counterpart, suggesting that for each zebrafish cell type, corresponding cell populations exist in the mammalian hippocampus (Fig. S5C). To infer the heterogeneity of cell identity within the zebrafish cell clusters, we also determined the cell type of the single corresponding, most similar murine cell for each zebrafish cell. We omitted cells that show only limited similarity to mammalian cells, identified by Hochgerner et al. (2018) (see Fig. S5C and Materials and Methods). The results show that cells forming the RG cluster in the adult zebrafish brain mainly correspond to various glial cell types in the murine brain i.e. astrocytes and radial glia-like neural stem cells (RGLs) of different maturation stages, neurogenic intermediate progenitor cells (nIPCs) with minor proportions corresponding to neuroblasts, OPCs and microglia. Zebrafish OPCs corresponded only to murine OPCs. Consistent with the pseudotime analysis, NBN.1 cells corresponded to neuroblasts and immature neurons of pyramidal, granule cell or GABAergic identity, while NBN.2 and MN cells mainly corresponded to mature neurons of GABAergic and pyramidal identity as well as juvenile granule cell neurons (Fig. 4C,D). In summary, these analyses reveal transcriptomic similarity of the neurogenic cell types of the adult zebrafish brain with those in the neurogenic niche of the developing and adult hippocampus. In particular, NBN.1 cells display pronounced similarity to neuroblasts and immature neurons, supporting their positioning as direct RG progeny in the pseudotime analysis.

Since a substantial proportion of NBN.1 cells showed similarity to neuroblast, which contain proliferating cells in mammalian adult neurogenic niches, we asked whether different subtypes of proliferating cells, e.g. radial glia, progenitors or neuroblasts (März et al. 2010a; Edelmann et al. 2013), are distributed along the pseudotime

trajectory in zebrafish. Using *ccnd1*, *mcm5* and *mki67* as markers for proliferating cells, proliferation was confined to the RG cluster and no proliferating cells were found elsewhere within the RG lineage (Fig. 5A), consistent with the pronounced prevalence of EdU^{+} cells in RGs at early EdU chase timepoints (see Fig 2B,C). Since *mcm5* and *mki67* expression is restricted to specific cell cycle phases (Ohtani et al., 1999; Sobecki et al., 2017), we used *ccnd1* as general proliferation marker to compare the transcriptome profile of ccnd1^{+}, proliferating RGs and ccnd1^{-} quiescent RGs. Apart from the expected enrichment of proliferation genes, such as *snrpd1*, *actl6a* and *mcm7* (Hiraiwa et al., 1997; Batra et al., 2012; Krasteva et al., 2012), neuronal fate determinants such as *ascl1a*, *sox4a* and marker genes of the NBN.1 clusters such as *tmsb* and *stmn1b* were significantly enriched in proliferating RGs (Fig. 5B; Fig. 3C; Table 1; Table 2). In contrast, classical RG marker such as *fabp7a*, *cx43*, *glula* (encoding glutamine synthase) and *s100b* were enriched in quiescent RG (Fig. 5B; Fig. 3C; Table 2). Substantiating a neurogenic commitment of proliferating RG, we found that 9% of the top100 marker genes of NBN.1 cells were also enriched in proliferating RG, while just one of them was found to be enriched in quiescent RG (Fig. S5B). Strikingly, out of the 4 neuronal fate determinants/neuronal genes (*ascl1a*, *sox4a, tmsb, stmn1b*) that were most substantially expressed in RGs (Table 2), 81% of proliferating RGs expressed 2 or more of them, while only 27% of quiescent RG did (Fig. 5C). With the exception of *ascl1a*, which was virtually confined to RG, all neuronal genes were further strongly enriched in NBN.1 cells, suggesting that RGs become committed to neurogenesis (indicated by consistent expression of neuronal fate determinants) and that many divisions from proliferating RGs are neurogenic. Taken together, we identify RG as the only proliferating cell type in the cell trajectory derived from *her4.1*-positive RG and provide strong evidence that most proliferating RG are committed to neurogenesis.

Next, we explored the gene expression changes upon the transition from RG to NBN.1 cells and towards MNs or NBN.2, respectively. Indeed, we observed waves of gene expression along the pseudotime ordering, identifying specific gene regulation along the differentiation trajectories. Consistent with the enrichment of the Notch target gene *her4.2* in proliferating RG (Fig. 5B), *her4.1* and *her 4.2* were increasingly expressed in RG that were advanced in the pseudotime trajectory (Fig. 5D,E). Further, panneuronal markers such as *elavl3* were consistently upregulated in all neuronal cell types compared to RG, while *tubb5* and *tmsb*, or *ebf3a* and *msi2b* were specifically seen in NBN.1 or NBN.2 clusters, respectively (Fig. 5D,E).

In conclusion, pseudotemporal ordering of RG, NBNs and MNs, identifies a differentiation trajectory from RG to NBN.1 cells, and reveals separate trajectories from NBN.1 towards NBN.2 cells or MNs, respectively. This conclusion is consistent with the comparison of zebrafish and murine neurogenic cell types, which reveals that RG, NBN.1 or NBN.2 and MN cells show transcriptomic similarities to cell types progressing in the known differentiation trajectory in this well-studied niche. Analysis of proliferation marker and neurogenic gene expression indicates that all analyzed proliferative cells in the her4.1-lineage are bona-fide RG, and that a neuronal transcription program is prevalent in proliferating RG. Finally, differential gene expression analysis along the trajectory confirms specific marker genes for the NBN.1, the NBN.2 and the MN population.

THE NBN.1 AND NBN.2 CLUSTERS FORM SPATIALLY DEFINED POPULATIONS OF NEWBORN NEURONS IN THE TELENCEPHALON AND DIENCEPHALON, RESPECTIVELY.

To identify factors that mediate the separation of the NBN.2 and the MN cluster as the two more differentiated neuronal cell clusters, we investigated the expression of key cell fate meditators for pan-neurogenic fate (sox4a, sox11a, *insm1a, insm1b, eomesa*), dorsal telencephalon glutamatergic fate *(neurod4, neurod1, neurod6a, neurod6b*), ventral forebrain GABAergic fate (*dlx1a, dlx2a, dlx5a*) and glutamatergic or GABAergic neuron identity (slc17a6a, slc17a6b, slc17a7a, gad1b, gad2) along the differentiation trajectory. Pan-neurogenic markers and *eomesa* were induced in differentiated RG, were abundantly expressed in the NBN1 cluster, and continued to be expressed, though in fewer cells, in both the NBN.2 and the MN cluster (Fig. 6A,B). Similarly, also the glutamatergic or GABAergic neuron markers were expressed by NBN.1, NBN.2 and MN cells. In contrast, the markers of dorsal telencephalon glutamatergic identity (magenta frame) and ventral telencephalon GABAergic identity (turquoise frame) were expressed in the NBN.1 and the MN cluster, but absent in the NBN.2 cluster, suggesting that the NBN.2 population of newborn neurons does not have telencephalic identity.

Next, we determined the localization of NBN.1 and NBN.2 cells in the adult forebrain using in-situ hybridization for their specific markers *tubb5* or *ebf3a, msi2b* and *tbr1b*, respectively (Fig. 3C, Fig. 5D,E). *tubb5* was expressed in the VZ and PVZ throughout the dorsal and ventral telencephalon, as well as the anterior, preoptic part of the diencephalon. Compared with the expression pattern of *mcherry* in the telencephalon of *her4.1:mcherry* fish, which is restricted to the VZ, the expression domain of tubb5 was notably extended into the PVZ, which is a known location for newborn neurons (Grandel et al., 2006; Ganz et al., 2010; Furlan et al., 2017) (Fig. 6C). These results

are consistent with the pseudotemporal positioning of *tubb5*-expressing NBN.1 cells as newborn neurons, most closely related to RG. In contrast, *ebf3a*-expression was absent in the telencephalon, but was found specifically in the ventral entopeduncular nucleus (vENT) in the lateral anterior diencephalon (Mueller and Guo, 2009; Turner et al., 2016). *msi2b* and *tbr1b* showed broader expression also in the dorsal telencephalon, but consistently labeled the vENT (Fig. 6C), suggesting that the NBN.2 population consists of vENT NBNs. Since adult neurogenesis was not reported in the vENT (Zupanc et al., 2005; Grandel et al., 2006), we investigated whether NBNs were located in the vENT. Adult fish were injected with EdU on three consecutive days and $EdU^+/HuC/D^+$ NBNs were analyzed 1 month after injection. As predicted, we found several EdU/HuC/D double-labeled neurons in the vENT (Fig. 6D), indicating that NBNs are added to this nucleus in adult stages. Thus, these results were consistent with our analysis of telencephalic marker expression (Fig. 6A) that suggested a location of NBN.2 cells outside of the telencephalon. Together, our spatial analysis shows that NBN.1 and NBN.2 cells are anatomically distinct populations of newborn neurons in the telencephalon and the diencephalon, respectively.

In conclusion, we have prospectively isolated RG, NBNs and MNs from the adult zebrafish forebrain, analyzed the kinetics of NBN generation and differentiation and performed unbiased, single-cell-resolution transcriptome analysis of these cells. This analysis revealed distinct clusters of NBNs (Fig. 6E), which correspond to NBNs in the telencephalon and diencephalon, respectively. In addition, we identified specific marker genes for NBNs, which may facilitate further research on this important cell type in the adult vertebrate brain.

DISCUSSION

The combination of lineage tracing and single cell sequencing is a powerful tool for dynamic analysis of somatic stem cell progeny and their role in tissue development, homeostasis and repair (Camp et al., 2018; Gerber et al., 2018; Kester and van Oudenaarden, 2018). Here, we have performed lineage tracing on the population level by using the inheritance of a fluorescent protein that is specifically expressed in RG to their progeny, similar to previous studies in the developing zebrafish telencephalon and regenerating adult retina (Fausett and Goldman, 2006; Furlan et al., 2017). We additionally used a fluorescent neuronal marker to identify NBNs derived from the RG lineage as cells that are double-positive for both markers. An EdU pulse-chase experiment demonstrated that the double-positive cells are specifically enriched for adult-generated neurons and provides evidence that this population is transient and dynamic, because they are enriched for EdU incorporating cells after a chase of 7 days, but not after 2 hours or 4 weeks, respectively. The results suggest that the double positive cells lose their mcherry fluorescence between 7 days and 4 weeks after their generation by proliferating precursors (likely RG) and are replaced by newly generated cells at the latter timepoint, consistent with our lineage tracing paradigm. The extent of RG proliferation measured by EdU incorporation is consistent with the frequency of proliferating RG in the literature (Dray et al., 2015). Also the persistence of her4.1-driven mcherry in the mcherry/GFP double-positive cells for up to 7 days is consistent with a previous *in vivo* imaging study, which reports inheritance of *gfap*:GFP in the differentiated daughter cells of RG for several days after division (Barbosa et al., 2015). Thus, these data verify our lineage tracing approach and provide important insights into the time line and kinetics of neurogenesis and neuronal differentiation. Finally, we were able to enumerate for the first time the extent of radial glia-derived newborn

neurons in the adult zebrafish forebrain, independent of thymidine analog administration. Using the *her4.1* promotor as a RG-specific driver, we find that circa 10% of sorted, live cells from the telencephalon are NBNs that still retain detectable levels of the RG-derived fluorescent marker. Our finding that *her4.1*:mcherry in the NBNs is detectable for several days after their generation from proliferating precursors (Fig. 2B,C) suggests that this NBN population is an accumulation of cells of different age since their generation, which likely ranges over one or two weeks, but less than 4 weeks. Consistently, our transcriptional analysis reveals a broad spectrum of differentiation states among NBNs, from NBN.1 cells that share substantial transcriptional overlap with RG (see Fig. 2C, S5A) to NBNs that form a common cluster with mature neurons (Fig. S2A). These results suggest that with our lineage tracing approach, we detect various differentiation states of NBNs, present at steady state in the uninjured telencephalon (Fig. 3B,C). The biological role of such a surprisingly high number of NBNs and the mechanisms of their integration are currently unknown, but our results pave the way for better investigation and manipulation of NBNs in the adult zebrafish brain. A recent report provided single cell transcriptional profiles of *her4.1*:GFP^{pos} radial glia and *her4.1*:GFP^{neg} neurons from the adult zebrafish telencephalon (Cosacak et al., 2019), but NBNs are likely under-represented in this analysis because her4.1:GFP^{low} cells were deliberately omitted from the analysis.

Using our lineage-tracing approach, we determined whether more committed proliferating progenitors are present among the RG progeny in the adult forebrain. This analysis, on the population level, showed that RG are the only proliferating cell population within the sampled cells of the *her4.1*-lineage (Fig. 5A). Our estimation of the frequency of proliferating versus quiescent RG matches the values reported by Dray et al (2015). We find that 11 out of 76 RG (14.5%) express the S/G2/M-phase

specific proliferation marker *mcm5* (Fig. 5A), corresponding to circa 15% of RG expressing the S/G2/M-marker PCNA or *mcm5*-driven EGFP on protein level (Dray et al., 2015). The data are consistent with our comparison of zebrafish and murine neurogenic cells, where a subset of RG correspond to intermediate neurogenic progenitors, the major proliferating population in murine hippocampal adult neurogenesis. They also align with previous clonal analysis of RG progeny (Kroehne et al., 2011; Rothenaigner et al., 2011), which also argue against a major role of non-radial glia cells for amplification of RG progeny in zebrafish. Such non-glial precursors, which were judged by absence of destabilized RFP (dRFP) expressed under the control of the *her4.1* promotor, but expression of *mcm5*-driven EGFP, have been recently proposed as quantitatively dominating proliferating cell type in the VZ/PVZ of the adult zebrafish telencephalon by live imaging *in vivo* (Dray et al., 2015). Since these progenitors miss classical glial markers, their lineage relationship with radial glia is currently unclear. Importantly, in our study, where mcherry is retained in RG progeny until 7days after division (Fig. 2B,C), virtually all proliferating *her4.1*:mcherry^{pos} cells showed a transcriptome profile consistent with RG identity (Fig. 5A,B). Similarly, recent sc-RNAseq studies in the adult zebrafish brain with higher cell throughput, only identified cells with transcriptomic profiles of radial glia as proliferating neurogenic precursors (Cosacak et al., 2019; Yu and He 2019). Our finding that a subset of zebrafish RG correspond to intermediate neurogenic progenitors, the major proliferating and amplifying population from the postnatal and adult murine hippocampus, while a NBN.1 subset corresponds to neuroblast, their direct progeny, support this view. Thus, our results argue against a direct lineage relationship of RG with these non-glial precursors, though we cannot exclude that the mcherry protein is diluted to undetectable levels in fast proliferating precursor progeny in radial glia, while it is still detectable in postmitotic neuronal progeny. We also find that gene expression

in proliferating RG is linked to neurogenesis, as expression of neurogenic cell fate determinants (*ascl1a*, *ascl1b* and *sox4a*) and NBN.1 marker genes (*tmsb* and *marcksb)* are enriched in proliferating RG (Fig. 5B). These data are consistent with *in vivo*-live imaging analyses of RG proliferation that found most RG divisions generate differentiated, non-RG progeny (Barbosa et al., 2015; Dray et al., 2015), which were in part identified as HuC/D^{pos} neurons (Barbosa et al., 2015). Thus, our study complements the *in vivo*-imaging of cellular behavior of neurogenic cell types in the adult zebrafish telencephalon with insights into the transcriptional regulation in quiescent, and proliferating RG and their progeny at single cell resolution.

Another currently mostly unsolved question concerns the type of NBNs that are found in the adult zebrafish brain. In the telencephalon, GABAergic interneurons and aminergic neurons were found among NBNs previously (Adolf et al., 2006; Grandel et al., 2006), but the identity of a major fraction of NBNs was still unclear. Using unbiased genome-wide analysis of neuronal cell type markers, we found that the majority of newborn neurons expressed the glutamatergic markers *slc16a6a* or *slc16a6b*, while a smaller fraction expressed the GABAergic markers *gad1b* or *gad2*. In particular, in the NBN.1 cluster, but not in the NBN.2 cluster, pallial fate determinants of the *neurod* gene family were co-expressed with glutamatergic markers (Fig. 4A,B), indicating a pallial glutamatergic identity. Thus, this study shows for the first time that zebrafish constitutively generate pallial glutamatergic neurons in adult stage, raising the possibility that this neuronal class can also be efficiently regenerated after brain injury.

Interestingly, we found a minor proportion of RG progeny that showed hallmarks of OPC identity, such as expression of *olig2*, *olig1*, *aplnrb*, *sox10* (Fig. 2B,C; Fig. S5A). OPCs with a very similar marker profile were also found in the juvenile zebrafish brain (Raj et al., 2018). Expression of marker genes for this population was also found prominently in sorted *olig2*:GFP^{pos} cells from the adult zebrafish spinal cord (Kroehne

et al., 2017), strongly suggesting that these cells are *bona fide* OPCs. Moreover, 28.6% of *olig2*:GFP^{pos} cells showed low levels of *her4.1*:mcherry, while numerous cells showed intermediate levels of mcherry and GFP (Fig. S4B,C). Given that more than 25% of *olig2*:GFP^{pos} cells are also positive for *her4.1*:mcherry, the double-positive cells are far too many to be accounted for by the small subpopulation of olig2:GFP^{pos} precursors in the midline of the ventral telencephalon (März et al., 2010b). The persistence of *her4.1*-driven mcherry fluorescence in these cells suggests that they are generated by RG in the adult zebrafish brain, in addition to the self-renewal capabilities of OPCs. Thus, here we provide first evidence for a possible generation of OPCs from RGs in the adult zebrafish brain. Whether specialized subsets of RGs for generation of neurons and OPCs exists is currently unclear, but future scRNASeq studies in the zebrafish brain with higher cell throughput will enable better clarification of this question.

Moreover, in addition to the NBN.1 population, which represents the nascent RG progeny, supported by pseudotime ordering, transcriptional overlap and comparison to corresponding mammalian cell types (Fig. 4A,C,D; Fig. S5A), we identify also two more mature populations of adult-generated neurons. One of these populations forms a common cluster with mature neurons that do not retain her4.1-driven mcherry fluorescence and expresses telencephalic identity markers such as *neurod* and *dlx* genes. The NBNs in this cluster are considered to be generated from adult RG within the last 4 weeks, based on the retention of *her4.1*:mcherry (Fig. 2B,C), but advanced in their maturation as many of them already express maturity markers such as sv2a (compare Fig. 3B and Fig. S2A). Within the MN cluster, cells expressing glutamatergic or GABAergic markers are found. Likely, the small number of analyzed cells in this cluster precludes the separation of these cell types into separate clusters, as found recently (Cosacak et al., 2019). The second, matured NBN.2 population lacks

telencephalic markers and consists mostly of glutamatergic neurons (Fig. 6B). Spatial analysis of marker genes identifies these NBNs as belonging to the vENT in the diencephalon, which is included in our analysis, because the anterior diencephalon cannot be surgically separated from the telencephalon on the whole-mount level. Together with our observation that EdU^{pos} NBNs are added to this nucleus in adult stages, this argues that these NBNs are likely derived from diencephalic RGs; further direct lineage tracing of diencephalic RGs is necessary to test this hypothesis.

Overall, we find that transcriptome analysis at single-cell resolution can sort out functionally and spatially defined subpopulations of RG progeny in the adult zebrafish brain. The insights presented here also highlight the heterogeneity of RG-reporter-positive cells in the adult zebrafish brain, and advocate for the use of multiple reporters to clearly define cell types.

Importantly, here we identified marker genes for functional subpopulations of NBNs, such as *tubb5* and *ebf3a* for the NBN.1 and NBN.2 population respectively. Another recent study also suggested a population of *tubb5*- and *neurod*-expressing cells as nascent, telencephalic neurons in the juvenile zebrafish brain (Raj et al., 2018). Our results are consistent with this conclusion, based on using lineage tracing, pseudotime-ordering and location analysis also in the adult brain. Identification of specific markers for NBNs – which are currently elusive – will greatly facilitate the study of their biology, because it enables the generation of transgenic tools for studying these cells, e.g. through CRISPR-Cas9-mediated generation of reporters, *Cre*ERT2 lines (Auer et al., 2014; Kesavan et al., 2017; Kesavan et al., 2018) or effector lines (NTR, dCas9-effectors, etc.).

MATERIAL AND METHODS

Zebrafish

Zebrafish were bred and maintained according to standard procedures. All animal procedures were approved by the Regierungspräsidium Dresden (permit AZ 24-9165.40-1/2007, 24-9165.40-1/2013-1, TVV 44/2017). Wild-type experimental fish were in the AB background. Fish were raised at a density of 50-60 fish/tank of 12 liters (Brand et al. 2002). Fish of either sex were used.

Transgenic fish lines

The *her4.1*:*mcherry*, the *elavl3*:*gfp* and the *olig2*:*gfp* lines were described previously (Kroehne et al., 2011; Park et al., 2000; Shin et al. 2003). For the generation of the *gfap* reporter line *Tg(gfap:nls-mcherry)*, the *gfap* promoter (Bernardos and Raymond, 2006) was PCR amplified (gfap-for 5′-gggccCACCTTTGGGATGTAGTGGAACGGG, gfap-rev 5′-ggccggccAGGAACGCTGGGACTCCATGGTGGA) flanked by *Apa*I and *Fse*I restriction sites that allowed substitution of the *her4.1* promoter of the *her4.1:mCherry-T2A-CreER*^{T2} plasmid (Kroehne et al., 2011). The mCherry reporter was PCR-amplified and flanked by unique restriction sites using the primers Cherry-Fse-for (atatGGCCGGCCgccaccatggctccaaagaagaagcgtaaggtaatggccatcatcaaggagttcatc) and Cherry-Asc-rev (cgccGGCGCGCCgaattaaaaaacctcccacacc). The nuclear localization sequence (nls) was introduced into the sequence by a 5' overhang of the PCR forward primer. The PCR product was subloned into the pCR2.1-TOPO vector. Next, the TOPO vector with the reporter and the *pTol(gfap:mcherry-T2A-CreERT2)*

construct were digested using the enzymes AscI and FseI and ligated to replace the mCherry-CreERT2 cassette with the nls-reporter. For germ line transformation, linearized plasmid DNA with transposase mRNA was injected into fertilized eggs (F0), raised to adulthood and crossed to AB wild-type fish as previously described (Kawakami et al., 2004). For the identification of transgenic fish, F1 embryos were examined under a fluorescent microscope and positive embryos were raised.

Tissue dissociation and cell sorting

Wild type or *her4.1*:*mcherry*;*elavl3*:*GFP* transgenic fish were sacrificed by an overdose (0.024%) of MS-222 (Sigma)(Brand et al., 2002) until cessation of opercular movement and transferred to ice-cold HBSS. The dorsal skull plates were removed using forceps, incisions were made caudal to the olfactory bulbs and rostral to the midbrain, and the intermittend telencephalon and anterior diencephalon was transferred to Eppendorf tubes. Of note, this dissection protocol will yield cells from both the telencephalon and the anterior diencephalon, as no clear anatomical separation exists between these two parts on the level of whole mount brain tissue. Single cell suspensions were prepared from single telencephali/anterior diencephali using the Neural Tissue Dissociation Kit (Miltenyi Bioscience) with enzymatic digestion at 28°C instead of 37°C to prevent heat stress of the zebrafish cells. Prior to sorting, all samples were passed through a 20 µm cell strainer to remove cell aggregates and Calcein Blue-AM (Thermo Bioscience) was added to a final concentration of 10 µM.

Cells expressing mCherry and GFP were detected on a LSR II cell sorter (BD Biosciences) after 488nm excitation and a bandpass-filter 564/42nm and 530/30nm, respectively. Calcein Blue was detected after 405nm excitation and a bandpass-filter 450/40nm. Forward and side scatter were used to select all events that show a

characteristic scatter profile of zebrafish brain cells. From this selection, all events that showed incorporation of the Calcein Blue were gated as living cells. Living cells were plotted for GFP and mCherry fluorescence to gate for the respective cell populations. Detection of all fluorescent samples was controlled against unstained WT cells. Single cells gated as RG (mcherry^{high}/GFP^{neg}), NBN (mcherry^{low}/GFP^{pos}) and MN (mcherry^{neg}/GFP^{pos}) were sorted into single cavities of 96 well plates containing 2 µl lysis buffer using index sort mode and a 100 µm nozzle. The samples were immediately frozen until preparation of sequencing libraries.

Analysis of EdU incorporation in fluorescent cell populations

For the analysis of EdU incorporation into the different cell types of forebrains from *her4.1*:*mcherry*;*elavl3*:*GFP* transgenic fish, 7 - 10 forebrains were pooled for one sample. At different times after EdU injection, forebrains were dissected, dissociated and processed for FACS as described above. Single cells gated as mcherry^{high}/GFP^{neg}, mcherry^{low}/GFP^{pos} and mcherry^{neg}/GFP^{pos} were sorted Eppendorf tubes containing 200 µL Click-IT fixative (Thermo) using a 100 µm nozzle. For the two mcherry^{pos} populations, 8.000 - 30.000 cells were sorted, for the mcherry^{neg}/GFP^{pos} population, sorting was stopped at 100.000 cells. Cells were incubated for 15 min in the dark and EdU was detected using the Click-IT Plus EdU AlexaFluor 647 Flow Cytometry Assay Kit (Thermo) according to the manufacturer´s instructions. After EdU detection, the cell pellet was resuspended in 200 µL HBSS (Thermo) including 10 µg/ml [w/v] and incubated for 10 min at room temperature to stain the DNA in cell nuclei. Cells that are positive for AlexaFluor 647-labeled EdU and/or Hoechst were detected on a LSR II cell sorter (BD Biosciences) using 633nm and 405 nm excitation and a bandpass-filter 660/20nm and 530/30nm, respectively.

Imaging flow cytometry

For imaging flow cytometry, dissected zebrafish forebrains were dissociated and processed as for conventional flow cytometry (see above). The dissociated cells were analyzed for reporter fluorescence (GFP and mcherry) and Calcein Blue as viability marker using an ImageStream X Mark II imaging flow cytometer (Amnis), after gating forebrain cells for singlets (aspect ratio versus area). Data were processed offline using IDEAS software (Amnis). At least 20 individual images of double-positive ($GFP^+/mcherry^+$) cells, mcherry only-positive cells ($GFP^-/mcherry^+$) , GFP only-positive cells ($GFP^+/mcherry^-$) and negative cells ($GFP^-/mcherry^-$) were analyzed and quantified for the appearance of GFP and DsRED within the same cell, doublets and cells with attached fluorescent debris.

RNA-sequencing

Cells were FACsorted into a 96 well plate containing 2 µl of nuclease free water with 0.2% Triton-X 100 and 4 U murine RNase Inhibitor (NEB), spun down and frozen at -80°C. After thawing the samples, 2 µl of a primer mix was added (5 mM dNTP (Invitrogen), 0.5 µM dT-primer*, 4 U RNase Inhibitor (NEB)). RNA was denatured for 3 minutes at 72°C and the reverse transcription was performed at 42°C for 90 min after filling up to 10 µl with RT buffer mix for a final concentration of 1x superscript II buffer (Invitrogen), 1 M betaine, 5 mM DTT, 6 mM $MgCl_2$, 1 µM TSO-primer*, 9 U RNase Inhibitor and 90 U Superscript II. After synthesis, the reverse transcriptase was inactivated at 70°C for 15 min. The cDNA was amplified using Kapa HiFi HotStart Readymix (Peqlab) at a final 1x concentration and 0.1 uM UP-primer under following cycling conditions: initial denaturation at 98°C for 3 min, 22 cycles [98°C 20 sec, 67°C 15 sec, 72°C 6 min] and final elongation at 72°C for 5 min. The amplified cDNA was

purified using 1x volume of hydrophobic Sera-Mag SpeedBeads (GE Healthcare) and DNA is eluted in 12 ul nuclease free water. The concentration of the samples was measured with a Tecan plate reader Infinite 200 pro in 384 well black flat bottom low volume plates (Corning) using AccuBlue Broad range chemistry (Biotium).

For library preparation 700 pg cDNA in 2 µl were mixed with 0.5 µl Tagment DNA Enzyme and 2.5 µl Tagment DNA Buffer (Nextera, Illumina) and tagmented at 55°C for 5 min. Subsequently, Illumina indices were added during PCR (72°C 3 min, 98°C 30 sec, 12 cycles [98°C 10 sec, 63°C 20 sec, 72°C 1 min], 72°C 5 min) with 1x concentrated KAPA Hifi HotStart Ready Mix and 0.7 uM dual indexing primers. After PCR, libraries were quantified with AccuBlue Broad range chemistry, equimolarly pooled and purified twice with 1x volume Sera-Mag SpeedBeads. This was followed by Illumina sequencing on a Nextseq500 aiming at an average sequencing depth of 0.5 mio reads per cell.

dT-primer: C6-aminolinker-AAGCAGTGGTATCAACGCAGAGTCGACTTTTTTTTTT TTTTTTTTTTTTTTTTTTTTVN, where N represents a random base and V any base beside thymidine;

TSO-primer: AAGCAGTGGTATCAACGCAGAGTACATrGrGrG, where rG stands for ribo-guanosine;

UP-primer: AAGCAGTGGTATCAACGCAGAGT

Computational analysis

Libraries were sequenced on an Illumina NextSeq 500 system, resulting in about 250,000 to 900,000 single end reads per cell. FastQC was used to examine quality of the reads after sequencing. Alignment of the reads to the GRCz10 reference, inclusive the 92 ERCC Spike-In transcripts, was done with GSNAP (v 2017-08-15) and Ensembl gene annotation version 87 was used to detect exon spanning reads. featureCounts (v1.5.3) was used with the same Ensembl annotation to count the uniquely aligned reads to the genes and to create a counts table.

To identify low quality cells, quality control metrics were calculated from the raw count matrix in R using the package scater (McCarthy et al. 2017). Only cells that had more 4.5 log10-transformed total reads, between 2.7 and 3.9 log10-transformed features with more than one read, less than 50% of the reads in the top 50 highest expressed genes, less than 20% reads from mitochondrial genes, less than 25% reads from spike-ins and for which more than 20% of the reads were mapped to the genome were used for further analysis. Using these criteria, from the 370 that were sequenced 264 cells (71%) were used for further analysis. Genes that were detected in less than 3 cells were not considered for downstream analysis.

Further analysis was performed using the scanpy package (master branch commit 623f0d4) (Wolf et al.2018). Using the scanpy function highly_variable_genes with max_mean set to 8.0, 5142 highly variable genes were identified from the log-transformed raw counts. Read counts were normalized using the deconvolution method implemented in the scran package (Lun, McCarthy, and Marioni 2016), log-transformed, and scaled to unit variance and zero mean. A principal component analysis was performed on the highly variable genes. t-SNE dimensionality reduction

was performed using the first 10 principal components (Ulyanov 2016). Based on the first 10 principal components, the diffusion map was calculated using a Gaussian kernel and sigma was implicitly determined by the distance to the 5 nearest neighbors (Haghverdi et al. 2015, Buettner, and Theis 2015; Coifman et al. 2005). For the clustering, the 10 nearest neighbor graph was computed based on the first 10 principal components (McInnes and Healy 2018). The neighborhood graph was used to perform Louvain clustering with the resolution parameter set to 0.5 (Blondel et al. 2008; Levine et al. 2015; Traag 2015). Marker genes were detected using logistic regression on the raw count matrix as implemented in scanpy. The identification of cell identities in these clusters was based on examining these marker genes. For further analysis, the OPCs were dropped and a principal component analysis was performed on the resulting count matrix. A diffusion map was calculated with the same parameters as above. Diffusion pseudotime was computed with scanpy's dpt function using the randomly chosen RG cell "RG-5_03_D09" as root (Haghverdi et al. 2015, Wolf et al., 2018b). To identify genes that mark the transitions between clusters, a pairwise differential expression analysis using a Wilcoxon rank-sum test was performed. For visualization of gene expression along diffusion pseudotime, a running average with a window width of 15 cells was computed.

Proliferative RGs were defined as those that had one or more reads of ccnd1. All other RGs were classified as non-proliferative. Differential expression analysis between the two groups was performed using a Wilcoxon rank-sum test. To examine the statistical significance of the over-representation of the top 100 marker genes for the NBN.1 cluster in the top 100 genes that are higher expressed in proliferative RGs compared to quiescent RGs a hypergeometric test was performed. From the 11 genes that were present in both, the top 100 marker genes for the NBN.1 cluster and the top 100 genes that are higher expressed in proliferative RGs, 4 genes associated with neurogenesis

were curated. For each cell, the number of expressed genes (>0 reads) among those 4 genes calculated. To test the statistical significance of the increase in the number of cells that express genes associated with neurogenesis in proliferative RGs a one-sided Wilcoxon rank-sum test was performed.

Comparison to murine cell types

For the combined cell type homology analysis, scanpy version 1.4.4 was used. Read counts and meta data on cell type identities from the developing mouse dentate gyrus were acquired from GEO accession number GSE104323. Read counts from zebrafish and mouse were normalized using the scanpy function normalize_per_gene and log-transformed using scanpy's log1p function. Next, the normalized count matrices for zebrafish and mouse were transformed into a count matrix for all orthologues gene pairs in the following way: A list of all pairs of orthologues genes between mouse (GRCm38.p6) and zebrafish (GRCz11) was downloaded from http://www.ensembl.org/biomart/martview/ (Database: Ensembl Genes 97; Dataset: Zebrafish genes (GRCz11); Filters: Orthologous Mouse Genes: Only; Attributes: Gene stable ID, Gene name, Mouse gene stable ID, Mouse gene name). It should be noted, that this is not a list of only one-to-one matches, i.e. a single species-specific gene can be contained in multiple pairs of orthologues genes. A cross-species count matrix was constructed in which each row corresponds to an orthologues gene pair and the columns correspond to the cells from both species. Let z_a^j denote the normalized expression of zebrafish gene *a* in zebrafish cell *j* and m_b^k denote the normalized expression of mouse gene *b* in mouse cell *k*. Then, the elements of this cross-species count matrix were assigned as

$$e^i_{a,b} = \begin{cases} z^i_a & \text{if cell } i \text{ is a zebrafish cell} \\ m^i_b & \text{if cell } i \text{ is a mouse cell} \end{cases}$$

for all mouse and zebrafish cells *i* and all orthologues gene pairs *a*, *b*. To align mouse and zebrafish data, batch correction was performed using scanpy's combat function using the species as the batch key. Highly variable orthologues gene pairs were selected using scanpy's highly_variable_genes with parameter flavor='cell_ranger'. A principal component analysis was performed on these highly variable orthologues gene pairs. Hierarchical clustering in the space of the first 50 principal components using a Pearson correlation distance was performed using scanpy's dendrogram function. For each zebrafish cell, the Pearson correlation distance to and the cell type of the nearest mouse cell in the space of the first 50 principal components was computed. To reduce the number of false positives, zebrafish cells with distances to mouse cells above the 66% quantile of the distance distribution were disregarded from the analysis.

Tissue preparation

Brains were exposed *in situ* and fixed at 4°C overnight in 2-4% paraformaldehyde /0.1M phosphate buffer (pH 7.5). They were washed twice with PB and transferred for decalcification and cryoprotection to 20% sucrose/20% EDTA in 0.1M phosphate buffer (pH 7.5). Brains were frozen in 7.5% gelatine/20% sucrose and cut at 14 µm. Sections were stored at −20°C.

In situ hybridization

RNA *in situ* hybridization on sections and on whole-mount brains and RNA probe generation was essentially performed as previously described (Ganz et al., 2012). Briefly, after defrosting at room temperature (RT), sections were rehydrated for 15 minutes in PBS with 0.3% TritonX (PBSTx) and incubated with the probe overnight at 62–65°C. Information on the antisense *in situ* riboprobe for *tbr1b* can be found in (Ganz et al., 2012). The *in situ* probe for *tubb5* was obtained from the Zebrafish Gene Collection (cDNA clone MGC:85895). Probes for ebf3a and msi2b were cloned from zebrafish embryonic cDNA with the following primers (*ebf3a*-F, CAGCCAGTGGAGATCGAAAGGACAG, *ebf3a*-R, TGCCGTAGGGAGAGTTCGCAGAGGA, *msi2b*-F, GTTAGCCATGGAGGGAGACG, *msi2b*-R, GCGTCTTGGAAAGGCAACTT). The sections were washed at 60–65°C in washing solution (1 × SSC, 50% deionized formamide) for 1 × 15 minutes and 2 × 30 minutes followed by 2 × 30 minutes MAB with 0.1% Tween-20 (MABT) washes. Sections were incubated for 1h at RT in 2% DIG-blocking reagent (Roche) and incubated with anti-DIG antibody (Roche Diagnostics, sheep, polyclonal, Fab fragments conjugated to alkaline phosphatase, #11093274910) diluted 1:4000 in 2% DIG-blocking reagent overnight at 4°C. Subsequently, sections were washed 4 × 20 minutes in MABT, equilibrated with staining buffer and stained with the substrate NBT/BCIP. The staining was controlled using a stereomicroscope. Finally, sections were washed 2 × 5 minutes in PBS, postfixed with 4% PFA for 20–30 minutes, washed again 2 × 10 minutes in PBS and mounted with 70% glycerol in PBS. All washing steps were performed on a shaker, all incubation steps in a humid chamber.

Immunohistochemistry and EdU detection

Immunohistochemistry was carried out as previously described (Kroehne et al., 2011). Briefly, for detection of HuC/D sections were subjected to antigen retrieval by 15 min incubation in 10 mM citrate buffer, pH 6.8. Primary and secondary antibodies were incubated in PBS with 0.3% Triton X-100 (PBS TX). Tissue sections were incubated in primary antibodies overnight at 4°C and secondary antibodies for 1h at room temperature. The slides were then washed in PBS TX and mounted. We used primary antibodies to HuC/D (Elavl3) (mouse, Thermo Fisher Scientific, A21271, 1/250). For primary antibody validation see: https://www.thermofisher.com/antibody/product/HuC-HuD-Antibody-clone-16A11-Monoclonal/A-21271. Alexa Fluor 633-conjugated secondary antibodies were used (Thermo Fisher Scientific, A-21050, A21422; 1/750). EdU was detected with the EdU Alexafluor 488 Plus Imaging Kit (Thermo Fisher Scientific, C10337) according to the manufacturer´s instructions.

EdU injection

Adult (6-12 months old) fish were anaesthetized with 0.01% MS-222 (Sigma) in fish water (Brand et al., 2002) until sedation and injected intraperitoneally with 20 µl of 5mg/ml EdU in PBS either for three times with 12 hours interinjection interval (for analysis of EdU incorporation in *her4.1:mcherry*; *elavl3*:*gfp*-double transgenic fish) or for three times on consecutive days (for detection of adult-generated neurons in the diencephalon), respectively. After further survival for one month, fish were sacrificed by overdose with 0.024% MS-222 (Sigma) in fish water (Brand et al., 2002) until cessation of opercular movement. Subsequently, brains were dissected and processed for FACS (for analysis of EdU incorporation in *her4.1:mcherry*; *elavl3*:*gfp*-double transgenic fish) or processed for cryosectioning (detection of adult-generated neurons in the diencephalon), respectively.

Image acquisition and processing

Images of brain sections, stained by in situ hybridization or immunofluorescence were imaged with a Zeiss Axioimager Z1 microscope with Apotome structured illumination to achieve optical sections in fluorescent images, using Zeiss Plan-Apochromat 5x/0.16 and Zeiss Plan-Apochromat 40x 0,95 objectives. To minimize crosstalk between the channels in multicolored specimens, sequential image acquisition was performed. The images were processed using ImageJ v.1.44 (http://rsb.info.nih.gov/ij/),) and Adobe Photoshop CC 2015. Figures were assembled using Adobe Illustrator CC 2015.

Statistics

For statistical analysis, n indicates the number of forebrain cell pools, where cells from 7-10 telencephali were pooled (EdU incorporation) or the number of single quiescent od proliferating RG cells (neurogenic commitment in proliferating RG). Statistical significance was determined using One Way ANOVA with Welch´s correction for heteroskedatic data followed by Bonferroni´s multiple comparison *post hoc* test (EdU incorporation) or one-sided Mann and Whitney U test (neurogenic commitment in proliferating RG), respectively. Statistical tests were performed with Graph Pad Prism 8. No animals or data points were excluded from the analyses. Cells in the single cell analysis were excluded based on pre-determined technical quality control parameters. No methods were used to pre-determine sample size or randomize group assignment.

ACKNOWLEDGEMENT

We thank Daniela Zöller for excellent technical assistance and Anne Gompf and Katja Bernhardt from the CMCB Flow Cytometry core facility for cell sorting and flow cytometry. The excellent work of our fish facility and the BIODIP Imaging Facility is acknowledged. The authors thank Volker Kröhne, Heiner Grandel and Fabrizio Olmeda for helpful discussions.

COMPETING INTERESTS

None declared.

AUTHOR CONTRIBUTION

CL and MB conceptualized and designed the project, and wrote the manuscript. CL performed experiments, supported by AM and VK and analyzed results. SRe performed single cell sequencing. FR, ML and SRu performed computational analysis. AW and AD provided research tools and methodology. All authors edited the manuscript.

FUNDING

This work was supported by grants to MB from the Deutsche Forschungsgemeinschaft (DFG FZT 111), European Union (European Research Council AdG Zf-BrainReg) and the German Excellence Initiative (EXC 168).

DATA AVAILABILITY

The sequencing data are deposited at GEO (accession number GSE137525) and can be viewed online under https://singlecell.broadinstitute.org/single cell/ study/SCP520. The source code for the computational analysis is available under https://github.com/fabianrost84/lange_single-cell_2019.

REFERENCES

Adolf, B., Chapouton, P., Lam, C. S., Topp, S., Tannhauser, B., Strahle, U., Gotz, M. and Bally-Cuif, L. (2006). Conserved and acquired features of adult neurogenesis in the zebrafish telencephalon. *Dev Biol* **295**, 278-293.

Aimone, J. B., Li, Y., Lee, S. W., Clemenson, G. D., Deng, W. and Gage, F. H. (2014). Regulation and function of adult neurogenesis: from genes to cognition. *Physiol Rev* **94**, 991-1026.

Alemany, A., Florescu, M., Baron, C. S., Peterson-Maduro, J. and van Oudenaarden, A. (2018). Whole-organism clone tracing using single-cell sequencing. *Nature* **556**, 108-112.

Alunni, A. and Bally-Cuif, L. (2016). A comparative view of regenerative neurogenesis in vertebrates. *Development* **143**, 741-753.

Alunni, A., Hermel, J. M., Heuze, A., Bourrat, F., Jamen, F. and Joly, J. S. (2010). Evidence for neural stem cells in the medaka optic tectum proliferation zones. *Dev Neurobiol* **70**, 693-713.

Amamoto, R., Huerta, V. G., Takahashi, E., Dai, G., Grant, A. K., Fu, Z. and Arlotta, P. (2016). Adult axolotls can regenerate original neuronal diversity in response to brain injury. *Elife* **5**.

Amir, E.-a. D., Davis, K. L., Tadmor, M. D., Simonds, E. F., Levine, J. H., Bendall, S. C., Shenfeld, D. K., Krishnaswamy, S., Nolan, G. P. and Pe'er, D. (2013). viSNE enables visualization of high dimensional single-cell data and reveals phenotypic heterogeneity of leukemia. *Nature Biotechnology* **31**, 545-552.

Auer, T. O., Duroure, K., De Cian, A., Concordet, J. P. and Del Bene, F. (2014). Highly efficient CRISPR/Cas9-mediated knock-in in zebrafish by homology-independent DNA repair. *Genome Res* **24**, 142-153.

Barbosa JS, Sanchez-Gonzalez R, Di Giaimo R, Baumgart EV, Theis FJ, Götz M and Ninkovic J. (2015). Neurodevelopment. Live imaging of adult neural stem cell behavior in the intact and injured zebrafish brain. Science **348**, 789-793.

Batra, R., Harder, N., Gogolin, S., Diessl, N., Soons, Z., Jager-Schmidt, C., Lawerenz, C., Eils, R., Rohr, K., Westermann, F., et al. (2012). Time-lapse imaging of neuroblastoma cells to determine cell fate upon gene knockdown. *PLoS One* **7**, e50988.

Baumgart, E. V., Barbosa, J. S., Bally-Cuif, L., Gotz, M. and Ninkovic, J. (2012). Stab wound injury of the zebrafish telencephalon: a model for comparative analysis of reactive gliosis. *Glia* **60**, 343-357.

Berg, D. A., Kirkham, M., Beljajeva, A., Knapp, D., Habermann, B., Ryge, J., Tanaka, E. M. and Simon, A. (2010). Efficient regeneration by activation of neurogenesis in homeostatically quiescent regions of the adult vertebrate brain. *Development* **137**, 4127-4134.

Bernardos, R. L. and Raymond, P. A. (2006). GFAP transgenic zebrafish. *Gene Expr Patterns* **6**, 1007-1013.

Bhardwaj, R. D., Curtis, M. A., Spalding, K. L., Buchholz, B. A., Fink, D., Bjork-Eriksson, T., Nordborg, C., Gage, F. H., Druid, H., Eriksson, P. S., et al. (2006). Neocortical neurogenesis in humans is restricted to development. *Proc Natl Acad Sci U S A* **103**, 12564-12568.

Blondel, V. D., Guillaume, J. L., Lambiotte, R. and Lefebvre, E. (2008). Fast unfolding of communities in large networks. *Journal of Statistical Mechanics- Theory and Experiment*.

Brand, M., Granato, M. and Nüsslein-Volhard C. (2002). Keeping and raising zebrafish. In Zebrafish (ed. C. Nüsslein-Volhard and R. Dahm), pp 7-37. Oxford, UK, Oxford University Press

Briggs, J. A., Weinreb, C., Wagner, D. E., Megason, S., Peshkin, L., Kirschner, M. W. and Klein, A. M. (2018). The dynamics of gene expression in vertebrate embryogenesis at single-cell resolution. *Science* **360**.

Camp, J. G., Wollny, D. and Treutlein, B. (2018). Single-cell genomics to guide human stem cell and tissue engineering. *Nat Methods* **15**, 661-667.

Coifman, R. R., Lafon, S., Lee, A. B., Maggioni, M., Nadler, B., Warner, F. and Zucker, S. W. (2005). Geometric diffusions as a tool for harmonic analysis and structure definition of data: Diffusion maps. *Proceedings of the National Academy of Sciences of the United States of America* **102**, 7426-7431.

Cosacak M. I., Bhattarai P., Reinhardt S., Petzold A., Dahl A., Zhang Y. and Kizil C. (2019). Single-Cell Transcriptomics Analyses of Neural Stem Cell Heterogeneity and Contextual Plasticity in a Zebrafish Brain Model of Amyloid Toxicity. *Cell Rep* **27**, 1307-1318.

Dray N., Bedu S., Vuillemin N., Alunni A., Coolen M., Krecsmarik M., Supatto W., Beaurepaire E. and Bally-Cuif L. (2015). Large-scale live imaging of adult neural stem cells in their endogenous niche. *Development* **142**, 3592-3600

Ekstrom, P., Johnsson, C. M. and Ohlin, L. M. (2001). Ventricular proliferation zones in the brain of an adult teleost fish and their relation to neuromeres and migration (secondary matrix) zones. *J Comp Neurol* **436**, 92-110.

Ernst, A. and Frisen, J. (2015). Adult neurogenesis in humans- common and unique traits in mammals. *PLoS Biol* **13**, e1002045.

Farrell, J. A., Wang, Y., Riesenfeld, S. J., Shekhar, K., Regev, A. and Schier, A. F. (2018). Single-cell reconstruction of developmental trajectories during zebrafish embryogenesis. *Science* **360**.

Fausett, B. V. and Goldman, D. (2006). A role for alpha1 tubulin-expressing Muller glia in regeneration of the injured zebrafish retina. *J Neurosci* **26**, 6303-6313.

Ferri, R. T. and Levitt, P. (1993). Cerebral cortical progenitors are fated to produce region-specific neuronal populations. *Cereb Cortex* **3**, 187-198.

Frisen, J. (2016). Neurogenesis and Gliogenesis in Nervous System Plasticity and Repair. *Annu Rev Cell Dev Biol* **32**, 127-141.

Furlan, G., Cuccioli, V., Vuillemin, N., Dirian, L., Muntasell, A. J., Coolen, M., Dray, N., Bedu, S., Houart, C., Beaurepaire, E., et al. (2017). Life-Long Neurogenic Activity of Individual Neural Stem Cells and Continuous Growth Establish an Outside-In Architecture in the Teleost Pallium. *Curr Biol* **27**, 3288-3301 e3283.

Ganz, J. and Brand, M. (2016). Adult Neurogenesis in Fish. *Cold Spring Harb Perspect Biol* **8**.

Ganz, J., Kaslin, J., Freudenreich, D., Machate, A., Geffarth, M. and Brand, M.

(2012). Subdivisions of the adult zebrafish subpallium by molecular marker analysis. *J Comp Neurol* **520**, 633-655.

Ganz, J., Kaslin, J., Hochmann, S., Freudenreich, D. and Brand, M. (2010). Heterogeneity and Fgf dependence of adult neural progenitors in the zebrafish telencephalon. *Glia* **58**, 1345-1363.

Gerber, T., Murawala, P., Knapp, D., Masselink, W., Schuez, M., Hermann, S., Gac-Santel, M., Nowoshilow, S., Kageyama, J., Khattak, S., et al. (2018). Single- cell analysis uncovers convergence of cell identities during axolotl limb regeneration. *Science* **362**.

Grandel, H. and Brand, M. (2013). Comparative aspects of adult neural stem cell activity in vertebrates. *Dev Genes Evol* **223**, 131-147.

Grandel, H., Kaslin, J., Ganz, J., Wenzel, I. and Brand, M. (2006). Neural stem cells and neurogenesis in the adult zebrafish brain: origin, proliferation dynamics, migration and cell fate. *Dev Biol* **295**, 263-277.

Haghverdi, L., Buettner, F. and Theis, F. J. (2015). Diffusion maps for high-dimensional single-cell analysis of differentiation data. *Bioinformatics* **31**, 2989- 2998.

Hiraiwa, A., Fujita, M., Nagasaka, T., Adachi, A., Ohashi, M. and Ishibashi, M. (1997). Immunolocalization of hCDC47 protein in normal and neoplastic human tissues and its relation to growth. *Int J Cancer* **74**, 180-184.

Hochgerner H., Zeisel A., Lönnerberg P., **Linnarsson** S. (2018). Conserved properties of dentate gyrus neurogenesis across postnatal development revealed by single-cell RNA sequencing. *Nat Neurosci* **21**, 290-299.

Huttner, H. B., Bergmann, O., Salehpour, M., Racz, A., Tatarishvili, J., Lindgren, E., Csonka, T., Csiba, L., Hortobagyi, T., Mehes, G., et al. (2014). The age and genomic integrity of neurons after cortical stroke in humans. *Nat Neurosci* **17**, 801-803.

Kaslin, J., Ganz, J. and Brand, M. (2008). Proliferation, neurogenesis and regeneration in the non-mammalian vertebrate brain. *Philos Trans R Soc Lond B Biol Sci* **363**, 101-122.

Kaslin, J., Kroehne, V., Ganz, J, Hans, S. and Brand M. (2017) Distinct roles of neuroepithelial-like and radial glia-like progenitor cells in cerebellar regeneration. *Development* **144**,1462-1471.

Kesavan, G., Chekuru, A., Machate, A. and Brand, M. (2017). CRISPR/Cas9-Mediated Zebrafish Knock-in as a Novel Strategy to Study Midbrain-Hindbrain Boundary Development. *Front Neuroanat* **11**, 52.

Kesavan, G., Hammer, J., Hans, S. and Brand, M. (2018). Targeted knock-in of CreER (T2) in zebrafish using CRISPR/Cas9. *Cell Tissue Res* **372**, 41-50.

Kester, L. and van Oudenaarden, A. (2018). Single-Cell Transcriptomics Meets Lineage Tracing. *Cell Stem Cell* **23**, 166-179.

Krasteva, V., Buscarlet, M., Diaz-Tellez, A., Bernard, M. A., Crabtree, G. R. and Lessard, J. A. (2012). The BAF53a subunit of SWI/SNF-like BAF complexes is essential for hemopoietic stem cell function. *Blood* **120**, 4720-4732.

Kroehne, V., Freudenreich, D., Hans, S., Kaslin, J. and Brand, M. (2011). Regeneration of the adult zebrafish brain from neurogenic radial glia-type progenitors. *Development* **138**, 4831-4841.

Kroehne, V., Kaslin, J. and Brand, M. (2009). Proliferation and cell fates during regeneration of the adult zebrafish brain. *Mech Dev* **126**, 291-292.

Kroehne, V., Tsata, V., Marrone, L., Froeb, C., Reinhardt, S., Gompf, A., Dahl, A., Sterneckert, J. and Reimer, M. M. (2017). Primary Spinal OPC Culture System from Adult Zebrafish to Study Oligodendrocyte Differentiation In Vitro. *Front Cell Neurosci* **11**, 284.

Kunze, A., Congreso, M. R., Hartmann, C., Wallraff-Beck, A., Huttmann, K., Bedner, P., Requardt, R., Seifert, G., Redecker, C., Willecke, K., et al. (2009). Connexin expression by radial glia-like cells is required for neurogenesis in the adult dentate gyrus. *Proc Natl Acad Sci U S A* **106**, 11336-11341.

Levine, Jacob H., Simonds, Erin F., Bendall, Sean C., Davis, Kara L., Amir, E.- ad D., Tadmor, Michelle D., Litvin, O., Fienberg, Harris G., Jager, A., Zunder, Eli R., et al. (2015). Data-Driven Phenotypic Dissection of AML Reveals Progenitor-like Cells that Correlate with Prognosis. *Cell* **162**, 184-197.

Li, X., Zhao, X., Fang, Y., Jiang, X., Duong, T., Fan, C., Huang, C. C. and Kain, S. R. (1998). Generation of destabilized green fluorescent protein as a transcription reporter. *J Biol Chem* **273**, 34970-34975.

Lun, A. T., McCarthy, D. J. and Marioni, J. C. (2016). A step-by-step workflow for low-level analysis of single-cell RNA-seq data with Bioconductor. *F1000Res* **5**, 2122.

Maaten, L. v. d. and Hinton, G. (2008). Visualizing Data using t-SNE. *Journal of Machine Learning Research* **9**, 2579-2605.

März, M., Chapouton, P., Diotel, N., Vaillant, C., Hesl, B., Takamiya, M., Lam, C. S., Kah, O., Bally-Cuif, L. and Strahle, U. (2010a). Heterogeneity in progenitor cell subtypes in the ventricular zone of the zebrafish adult telencephalon. *Glia* **58**, 870-888.

März M., Schmidt R., Rastegar S. and, Strahle U. (2010b). Expression of the transcription factor Olig2 in proliferating cells in the adult zebrafish telencephalon. *Dev Dyn* **239**, 3336- 3349.

März, M., Schmidt, R., Rastegar, S. and Strahle, U. (2011). Regenerative response following stab injury in the adult zebrafish telencephalon. *Dev Dyn* **240**, 2221- 2231.

McCarthy, D. J., Campbell, K. R., Lun, A. T. and Wills, Q. F. (2017). Scater: pre-processing, quality control, normalization and visualization of single-cell RNA- seq data in R. *Bioinformatics* **33**, 1179-1186.

McInnes, L. and Healy, J. (2018). UMAP: Uniform Manifold Approximation and Projection for Dimension Reduction. *arXiv:1802.03426 [cs, stat]*.

Mueller, T. and Guo, S. (2009). The distribution of GAD67-mRNA in the adult zebrafish (teleost) forebrain reveals a prosomeric pattern and suggests previously unidentified homologies to tetrapods. *J Comp Neurol* **516**, 553-568.

Ohab, J. J., Fleming, S., Blesch, A. and Carmichael, S. T. (2006). A neurovascular niche for neurogenesis after stroke. *J Neurosci* **26**, 13007-13016.

Park, H. C., Kim, C. H., Bae, Y. K., Yeo, S. Y., Kim, S. H., Hong, S. K., Shin, J., Yoo, K. W., Hibi, M., Hirano, T., et al. (2000). Analysis of upstream elements in the HuC promoter leads to the establishment of transgenic zebrafish with fluorescent neurons. *Dev Biol* **227**, 279-293.

Park, H. C., Shin, J., Roberts, R. K. and Appel, B. (2007). An olig2 reporter gene marks oligodendrocyte precursors in the postembryonic spinal cord of zebrafish. *Dev Dyn* **236**, 3402-3407.

Picelli, S., Faridani, O. R., Bjorklund, A. K., Winberg, G., Sagasser, S. and Sandberg, R. (2014). Full-length RNA-seq from single cells using Smart-seq2. *Nat Protoc* **9**, 171-181.

Raj, B., Wagner, D. E., McKenna, A., Pandey, S., Klein, A. M., Shendure, J., Gagnon, J. A. and Schier, A. F. (2018). Simultaneous single-cell profiling of lineages and cell types in the vertebrate brain. *Nat Biotechnol* **36**, 442-450.

Reimer, M. M., Sorensen, I., Kuscha, V., Frank, R. E., Liu, C., Becker, C. G. and Becker, T. (2008). Motor neuron regeneration in adult zebrafish. *J Neurosci* **28**, 8510-8516.

Rodriguez Viales, R., Diotel, N., Ferg, M., Armant, O., Eich, J., Alunni, A., Marz, M., Bally-Cuif, L., Rastegar, S. and Strahle, U. (2015). The helix-loop-helix protein id1 controls stem cell proliferation during regenerative neurogenesis in the adult zebrafish telencephalon. *Stem Cells* **33**, 892-903.

Rothenaigner, I., Krecsmarik, M., Hayes, J. A., Bahn, B., Lepier, A., Fortin, G., Gotz, M., Jagasia, R. and Bally-Cuif, L. (2011). Clonal analysis by distinct viral vectors identifies bona fide neural stem cells in the adult zebrafish telencephalon and characterizes their division properties and fate. *Development* **138**, 1459-1469.

Saha, B., Peron, S., Murray, K., Jaber, M. and Gaillard, A. (2013). Cortical lesion stimulates adult subventricular zone neural progenitor cell proliferation and migration to the site of injury. *Stem Cell Res* **11**, 965-977.

Skaggs, K., Goldman, D. and Parent, J. M. (2014). Excitotoxic brain injury in adult zebrafish stimulates neurogenesis and long-distance neuronal integration. *Glia* **62**, 2061-2079.

Shin J., Park H.C., Topczewska J.M., Mawdsley D.J.and Appel B. (2003). Neural cell fate analysis in zebrafish using olig2 BAC transgenics. *Methods Cell Sc*i **25**, 7-14

Spanjaard, B., Hu, B., Mitic, N., Olivares-Chauvet, P., Janjuha, S., Ninov, N. and Junker, J. P. (2018). Simultaneous lineage tracing and cell-type identification using CRISPR-Cas9-induced genetic scars. *Nat Biotechnol* **36**, 469-473.

Traag, V. A. (2015). louvain-igraph: v0.5.3. Zenodo.

Tsata V, Kroehne V, Reinhardt S, El-Armouche A, Brand M, Wagner M and Reimer MM. (2019). Electrophysiological Properties of Adult Zebrafish Oligodendrocyte Progenitor Cells. *Front Cell Neurosci*, doi: 10.3389/fncel.2019.00102

Turner, K. J., Hawkins, T. A., Yanez, J., Anadon, R., Wilson, S. W. and Folgueira, M. (2016). Afferent Connectivity of the Zebrafish Habenulae. *Front Neural Circuits* **10**, 30.

Ulyanov, D. (2018). Multicore-TSNE. https://github.com/DmitryUlyanov/Multicore-TSNE.

Wagner, D. E., Weinreb, C., Collins, Z. M., Briggs, J. A., Megason, S. G. and Klein, A. M. (2018). Single-cell mapping of gene expression landscapes and lineage in the zebrafish embryo. *Science* **360**, 981-987.

Wolf, F. A., Angerer, P. and Theis, F. J. (2018a). SCANPY: large-scale single-cell gene expression data analysis. *Genome Biology* **19**.

Wolf, F. A., Hamey, F., Plass, M., Solana, J., Dahlin, J. S., Gottgens, B., Rajewsky, N., Simon, L. and Theis, F. J. (2018b). Graph abstraction reconciles clustering with trajectory inference through a topology preserving map of single cells. *bioRxiv*, 208819.

Yu S. and He J. (2019). Stochastic cell-cycle entry and cell-state-dependent fate outputs of injury-reactivated tectal radial glia in zebrafish. *eLife,* doi:10.7554/eLife.48660

Zhong, L. and Gerges, N. Z. (2012). Neurogranin targets calmodulin and lowers the threshold for the induction of long-term potentiation. *PLoS One* **7**, e41275.

Zupanc, G. K., Hinsch, K. and Gage, F. H. (2005). Proliferation, migration, neuronal differentiation, and long-term survival of new cells in the adult zebrafish brain. *J Comp Neurol* **488**, 290-319.

FIGURES

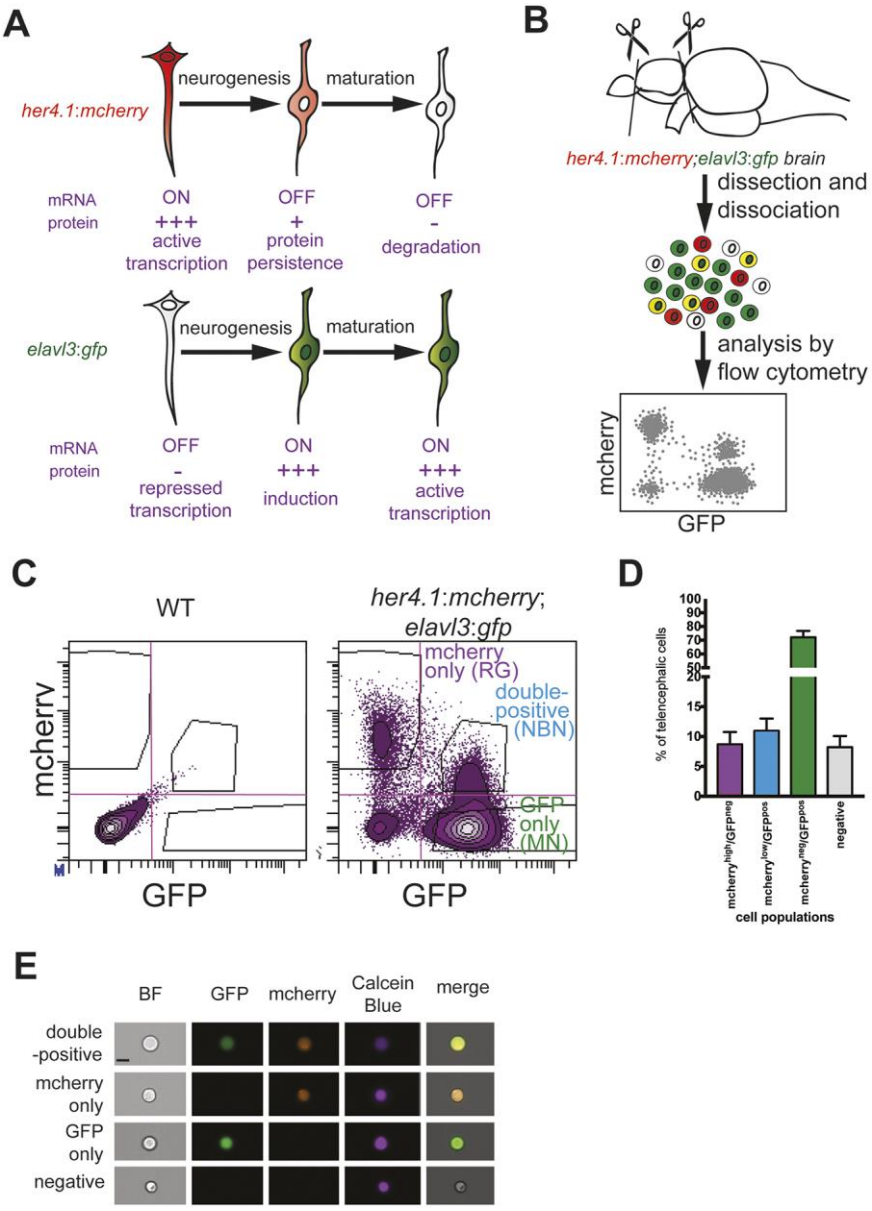

Figure 1

(A) Model for the lineage-trace paradigm: NBNs stop to transcribe *her4.1*-driven *mcherry*, but inherit the protein from their RG precursors (top). At the same time, NBNs induce transcription of the neuronal marker *elavl3*:*gfp* (bottom), allowing to identify NBNs as mcherry/GFP-double positive cells in double reporter fish. (B) Scheme of the analytical workflow: forebrains are removed from double reporter fish, dissociated and cell types are analyzed by flow cytometry. (C) Representative FACS-plots showing

forebrain cells from WT (left) and *her4.1*:*mcherry*;*elavl3*:*gfp* double reporter fish (right). Note the clearly separated populations of mcherry^{high}/GFP^{neg} RG and mcherry^{low}/GFP^{pos} NBNs. (D) Quantification of cells in the 4 quadrants shown in (C) revealing that NBNs can be found in a frequency comparable to RGs and represent circa 10% of forebrain cells. N=5; data are presented as mean±SEM. (E) Representative single cells imaged in flow cytometry for mcherry^{pos}/GFP^{pos} (top), mcherry^{pos}/GFP^{neg} (middle, top), mcherry^{neg}/GFP^{neg} (middle,bottom) and , mcherry^{neg}/GFP^{neg} (bottom). At least 20 cells were analyzed and no doublets were seen, excluding that double-positive cells represent doublets. Scale bar = 7 µm.

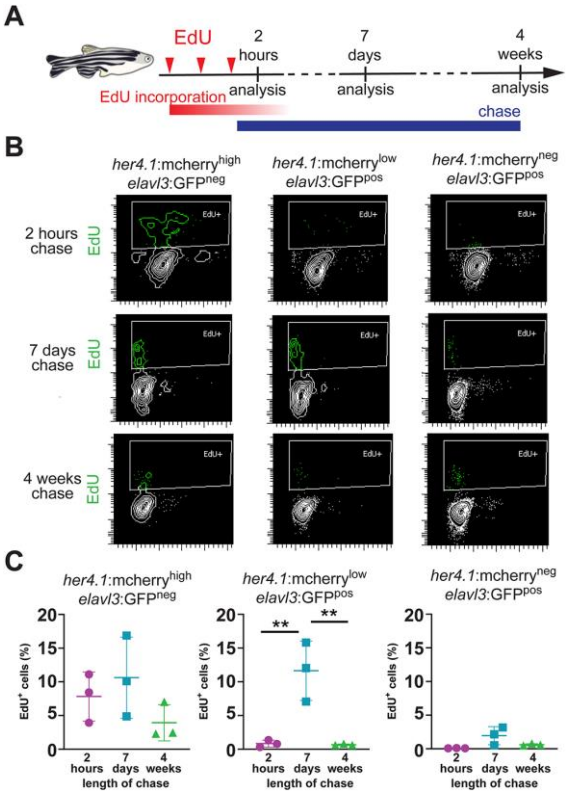

Figure 2

(A) Scheme of experimental design indicating the timing of EdU injections (red arrowheads), EdU incorporation (red bar), EdU chase (blue bar) and analysis timepoints after the last EdU injection. (B) Flow cytometry plots showing EdU (green) incorporation in sorted *her4.1*:mcherry^{high}/*elavl3*:GFP^{neg} cells (left), *her4.1*:mcherry^{low}/*elavl3*:GFP^{pos} cells (middle) and *her4.1*:mcherry^{neg}/*elavl3*:GFP^{pos} cells (right) after 2 hours (top), 7 days (middle) or 4 weeks (bottom) of chase. Note the robust EdU labeling in *her4.1*:mcherry^{low}/*elavl3*:GFP^{pos} after 7 days, but not 2 hours or 4 weeks chase. (C) Quantification of EdU labeling *her4.1*:mcherry^{high}/*elavl3*:GFP^{neg} cells (left), *her4.1*:mcherry^{low}/*elavl3*:GFP^{pos} cells (middle) and *her4.1*:mcherry^{neg}/*elavl3*:GFP^{pos} cells (right) after 2 hours (magenta), 7 days (petrol) or 4 weeks (green). Shown are single data points; n=3; mean±SEM are indicated. Significance: **= p< 0.01 by One way ANOVA and Bonferroni *post hoc* test.

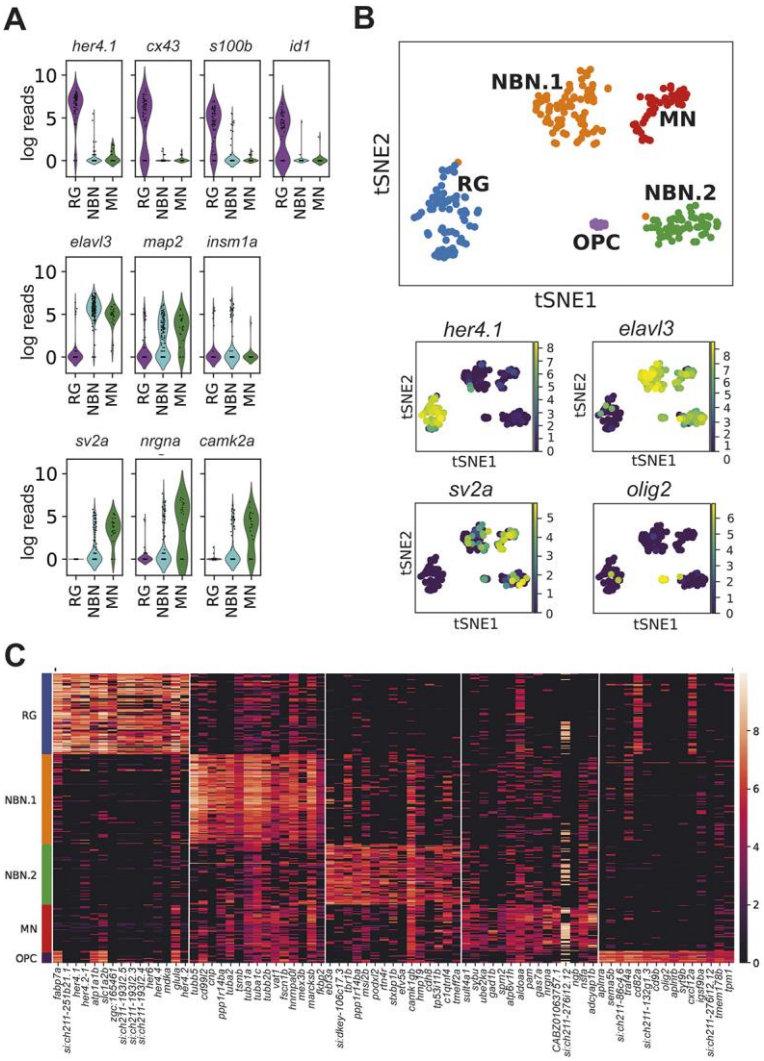

Figure 3

(A) Violin plots showing the expression of known radial glia markers (top); pan-neuronal markers (middle, left and middle), and early neurogenic fate marker (middle right) and markers of mature, synaptically integrated neurons (bottom). (B) tSNE plot revealing 5 different cluster from a total of 264 RG, NBN and MN cells (top). The cell number per cluster is: RG (76 cells), NBN.1(80 cells), NBN.2 (54 cells), MN (44 cells), OPC (10 cells). Smaller panels in middle and bottom show expression of characteristic marker genes that separate the different clusters. (C) Heat map with the top 15 cluster-specific genes for the 5 identified clusters.

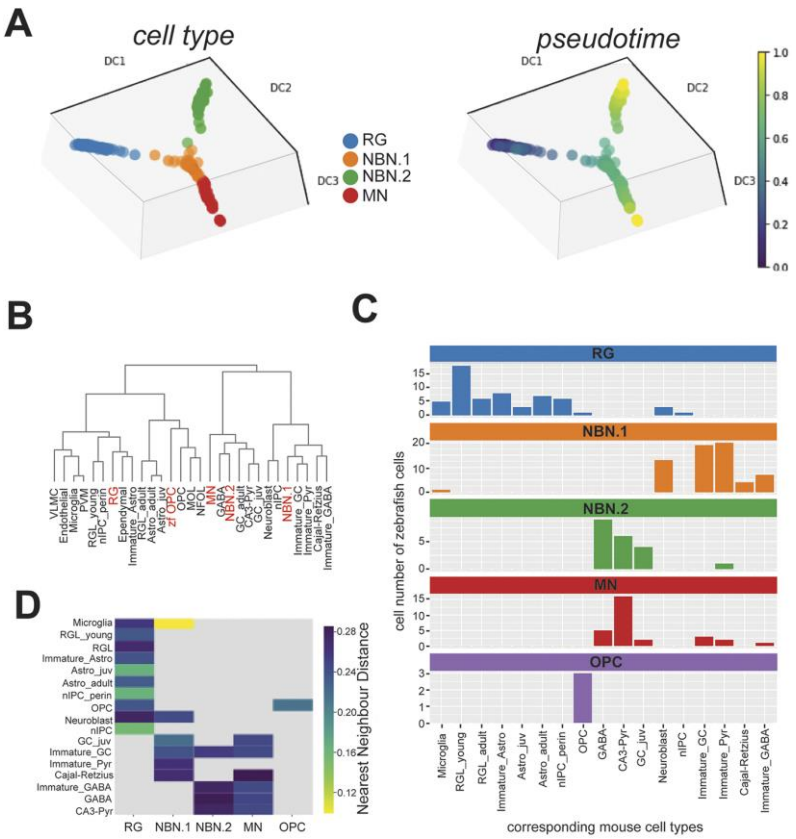

Figure 4

(A) Lineage trajectory analysis of single-cell RNAseq data from RG, NBNs and MNs of the adult zebrafish forebrain. Color coding corresponds to the different cell clusters identified in Figure 2B. (left) or indicates the pseudotime progression (right). (B) Unbiased hierarchical clustering of transcriptome profile from zebrafish cell clusters (red) with cell types from the developing and adult murine hippocampus (black), showing dispersed co-distribution of zebrafish cell clusters with related mammalian cell types. (C) Quantification of distribution of zebrafish cell clusters over the different corresponding murine cell types for RG (blue), NBN.1 cells (orange), NBN.2 cells (green), MNs (red) and OPCs (purple). Bars specify the number of zebrafish cells (on y-axis) corresponding to the indicated murine cell type (on x-axis). (D) Heatmap depicting the similarity of zebrafish cell clusters with their corresponding murine cell types based on the k-nearest neighbor distance. Lower distances indicate higher similarities.

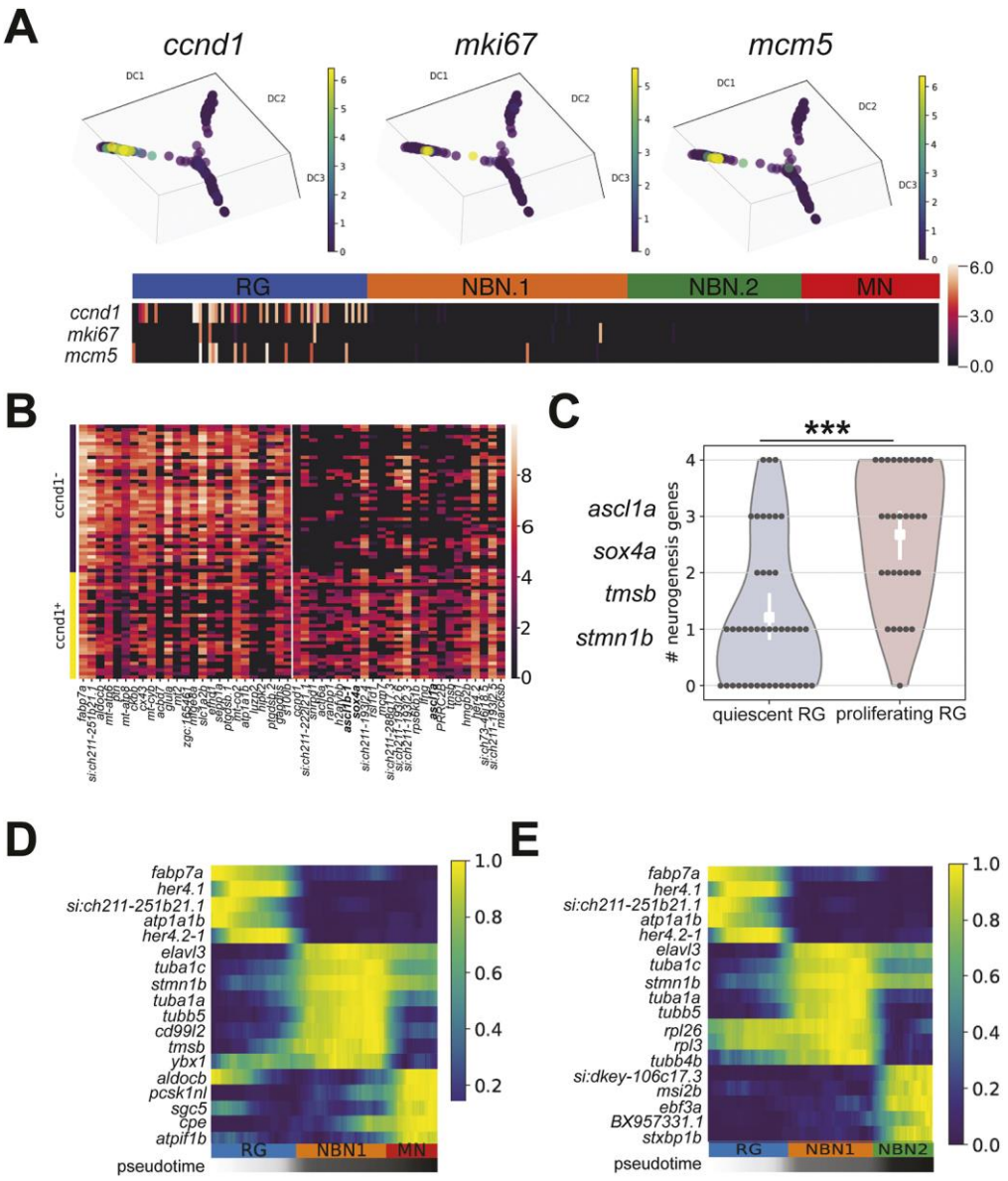

Figure 5

(A) Expression pattern of the proliferation markers *ccnd1* (top left), *mki67* (top middle) and *mcm5* (top right) along the trajectory path of RG differentiation. A heatmap indicating the co-expression of these genes in RG is shown at the bottom. (B) Heatmap showing differentially expressed genes in *ccnd1*$^{-}$, quiescent RG and *ccnd1*$^{+}$ proliferating RG. Note the enrichment of classical RG markers in quiescent RG (left, bold) and neurogenic fate determinants and NBN.1 marker genes in proliferating RG (right, bold), respectively. (C) Violin plot showing cumulative expression of the 4 most

widely expressed neurogenic fate determinants and neuronal genes (shown left) in quiescent (grey,) and proliferating (red) RG. Dots represent cells expressing the indicated number of genes. n=45 or 31, respectively. ***=p<0.001 by Mann and Whitney U-test. (D,E) Heatmap showing gene expression dynamics of differentially expressed genes along the differentiation trajectory from RG to MNs (D) or RG to NBN.2 cells (E), respectively. Genes (row) are clustered and cells (column) are ordered according to the pseudotime development. Note the specific expression of *tubb5* in the NBN.1 and of *ebf3a* and *msi2b* in the NBN.2 cluster.

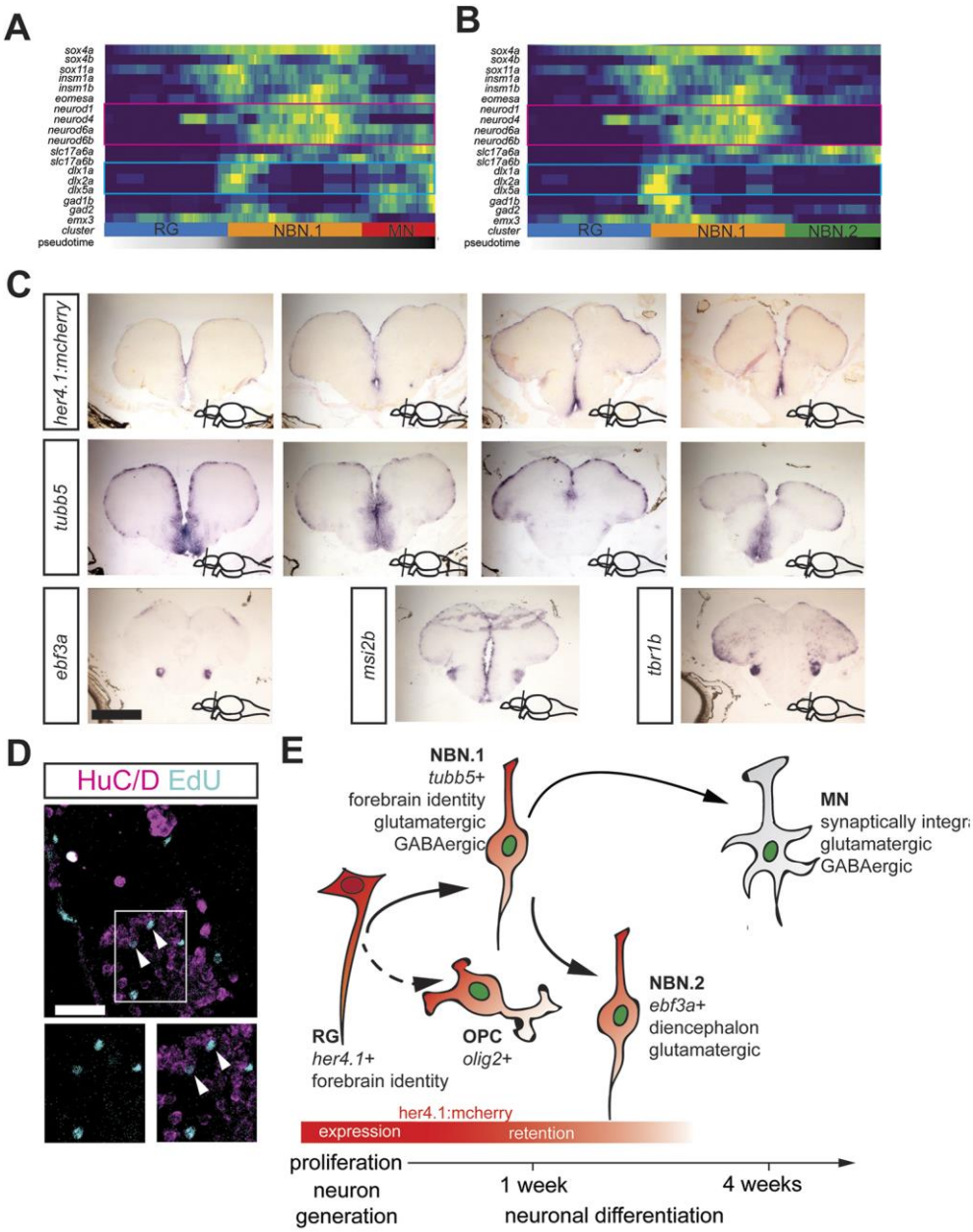

Figure 6

(A,B) Heatmap showing gene expression dynamics of proliferation markers, Notch targets, neurogenic fate determinants, telencephalic identity markers and neuronal subtype markers along the differentiation trajectory from RG to MNs (A) or RG to NBN.2 cells (B), respectively. Genes (row) are clustered and cells (column) are ordered according to the pseudotime development. Magenta and turquoise frames mark identity markers for dorsal or ventral telencephalon, respectively. (C) In situ hybridization for *mcherry* in *her4.1*:*mcherry* reporter fish (top), the NBN.1 marker *tubb5*

(middle) and the NBN.2 markers *ebf3a*, *msi2b* and *tbr1b* (bottom) in WT fish. Note the consistent expression of NBN.2 markers in the lateral diencephalon. The rostro-caudal level of the section is indicated in the bottom right corner. (D) Optical section of immunostaining for the neuronal markers HuC/D (magenta) and EdU labeling (turquoise) in the vENT, indicating the localization of NBNs. (E) Schematic representation of the resulting model from this study. Scale bar = 200 µm (C) or 20 µm, respectively.

RG	score	NBN.1	score	NBN.2	score	MN	score	OPC	score
fabp7a	0,026	*tubb5*	0,031	*ebf3a*	0,035	*sult4a1*	0,014	*aplnra*	0,013
si:ch211-251b21.1	0,025	*cd99l2*	0,025	*si:dkey-106c17.3*	0,027	*pam*	0,013	*sema5a*	0,011
her4.1	0,024	*pppr14ba*	0,022	*tbr1b*	0,026	*si:ch211-276i12.12*	0,013	*si:ch211-286c4.6*	0,011
atp1a1b	0,020	*cnp*	0,019	*msi2b*	0,025	*gad1b*	0,013	*traf4a*	0,011
her4.2-1	0,020	*tubb2b*	0,017	*podxl2*	0,023	*atp6v1h*	0,012	*cd82a*	0,011
slc1a2b	0,020	*mex3b*	0,016	*rtn4r*	0,022	*tspan18a*	0,012	*si:ch211-132g1.3*	0,011
zgc:165461	0,019	*hnrnpa0l*	0,016	*stxbp1b*	0,021	*diras1a*	0,012	*cd9b*	0,010
si:ch211-193l2.5	0,019	*vim*	0,015	*camk1gb*	0,020	*sybu*	0,011	*olig2*	0,010
si:ch211-193l2.3	0,019	*zfpm2a*	0,015	*etv5a*	0,019	*pfkpa*	0,011	*aplnrb*	0,010
si:ch211-193l2.4	0,019	*elavl3*	0,014	*BX957331.1*	0,016	*eef2l2*	0,011	*syt9b*	0,009
her6	0,019	*ahsa1b*	0,014	*PCP4L1 (1 of many)*	0,015	*si:dkey-35i13.1*	0,011	*cxcl12a*	0,009
her4.4	0,018	*tuba2*	0,014	*oxct1a*	0,014	*nrgna*	0,011	*igsf9ba*	0,009
mdka	0,017	*zgc:153426*	0,014	*tp53i11b*	0,014	*ngb*	0,011	*si:busm1-57f23.1*	0,009
glula	0,017	*tubb4b*	0,013	*cdh8*	0,013	*ube2ka*	0,011	*tmem178b*	0,009
her4.2	0,017	*tmsb*	0,013	*atp1b1b*	0,013	*eno2*	0,010	*slc1a2b*	0,009
slc1a3b	0,017	*hspa5*	0,013	*tmeff2a*	0,013	*pcsk1nl*	0,010	*TPM1*	0,009
s100b	0,016	*syt4*	0,013	*si:ch211-202a12.4*	0,013	*cacna2d2a*	0,010	*lrrn1*	0,009
cx43	0,016	*tuba1a*	0,013	*c1qtnf4*	0,013	*atpif1b*	0,010	*atp1a1b*	0,009
her15.2	0,016	*fscn1a*	0,012	*khdrbs2*	0,012	*sprn2*	0,010	*si:ch211-137a8.4*	0,008
her9	0,015	*slc38a2*	0,012	*meis1b*	0,012	*ppp3cb*	0,010	*olig1*	0,008
her15.1	0,015	*eef1g*	0,012	*hmp19*	0,012	*SMIM18*	0,010	*rgcc*	0,008
sepp1a	0,015	*dpysl5a*	0,012	*uncx4.1*	0,012	*fam107b*	0,010	*bcan*	0,008
atp1b4	0,014	*dnajb1b*	0,012	*si:dkey-238f9.1*	0,012	*sulf2b*	0,010	*dscamb*	0,008
dla	0,014	*kdm6bb*	0,012	*zfhx4*	0,012	*gas7a*	0,009	*fabp7a*	0,008
fads2	0,014	*prdm8b*	0,012	*edil3a*	0,012	*spon1a*	0,009	*cd63*	0,008
efhd1	0,013	*rcan1a*	0,012	*uncx*	0,011	*sh3gl2*	0,009	*sox10*	0,008
cox4i2	0,013	*si:ch73-281n10.2*	0,012	*snap25b*	0,011	*fxyd6*	0,009	*nptx1l*	0,008
ptn	0,012	*jun*	0,012	*elavl4*	0,011	*tspan2a*	0,009	*taok3a*	0,008
lix1	0,012	*zc4h2*	0,012	*bhlhe40*	0,011	*atp6v0cb*	0,009	*scg3*	0,008
s1pr1	0,012	*rtn1b*	0,012	*ptprn2*	0,011	*gabrg2*	0,009	*usp3*	0,008

Table 1: marker genes for the different clusters

quiescent RG		proliferating RG	
gene	score	gene	score
fabp7a	4,519	ccnd1	7,302
si:ch211-251b21.1	4,421	si:ch211-222l21.1	4,054
aldocb	4,388	snrpd1	3,391
mt-atp6	4,328	actl6a	3,298
ptn	4,300	ranbp1	3,292
mt-atp8	4,163	h2afvb	3,232
ckbb	4,092	ascl1b-1	3,183
cx43	4,092	sox4a	3,073
mt-cyb	4,076	si:ch211-193l2.4	2,985
acbd7	4,010	rsl1d1	2,953
glula	3,851	mcm7	2,903
mt2	3,824	si:ch211-288g17.3	2,892
fgfbp3	3,681	si:ch211-193l2.6	2,794
mfge8a	3,659	si:ch211-193l2.3	2,783
slc1a2b	3,654	rps6kb1b	2,766
efhd1	3,637	lfng	2,744
sepp1a	3,594	ascl1a	2,739
ptgdsb.1	3,583	PRRC2B	2,728
mt-co2	3,550	tmsb	2,723
atp1a1b	3,489	tcp1	2,723
luzp2	3,484	hmgb2b	2,712
hipk2	3,478	her4.2	2,706
ptgdsb.2	3,446	si:ch73-46j18.5	2,690
gapdhs	3,435	si:ch211-193l2.5	2,662
s100b	3,418	marcksb	2,657
mt-co3	3,369	hmga1a	2,635
slc4a4a	3,336	cct4	2,618
sdcbp2	3,325	ccnd2a	2,613
slc6a11b	3,309	nap1l1	2,607
zgc:153704	3,237	srsf2a	2,591
tegt	3,205	ddx21	2,531
psap	3,122	si:ch211156b7.4	2,525
s1pr1	3,095	hnrnpabb	2,492
lgals2a	3,040	arrdc3b	2,481
gmnn	3,035	mibp2	2,471
b2ml	2,991	boc	2,460
hepacama	2,964	snrpd3l	2,454
mt-nd1	2,936	her4.4	2,449
mgll	2,925	dla	2,438
atp1b4	2,914	kdm6ba	2,432
anxa11b	2,887	slc6a15	2,405
drg3a	2,887	her15.1	2,399
itm2ba	2,854	stmn1b	2,399
ppap2	2,827	rps23	2,394
mt-nd2	2,777	ran	2,361
cxcl12a	2,772	h3f3a	2,361
grm2b	2,739	rpl22l1	2,350

Table 2: Differentially expressed genes between quiescent and proliferating RG.

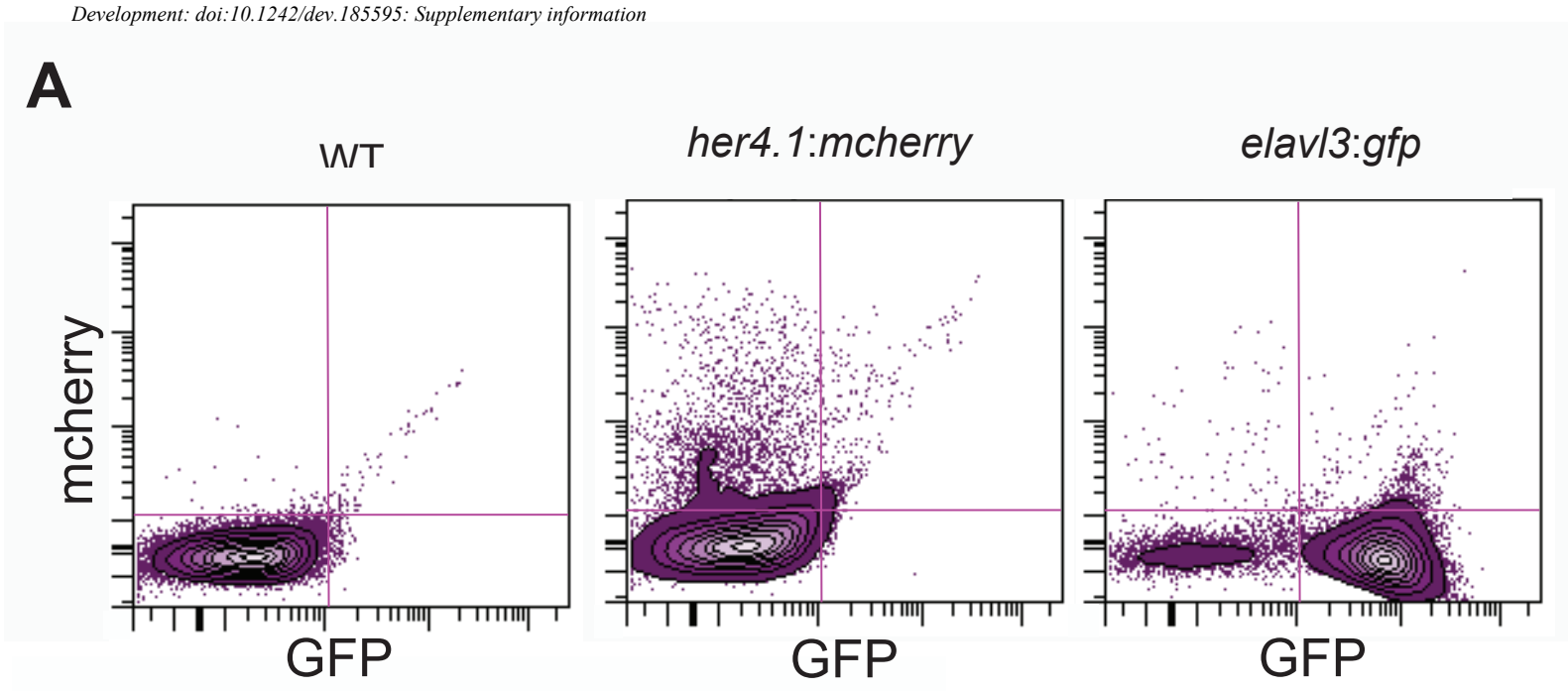
A
WT
her4.1:mcherry
elavl3:gfp
mcherry
GFP
GFP
GFP

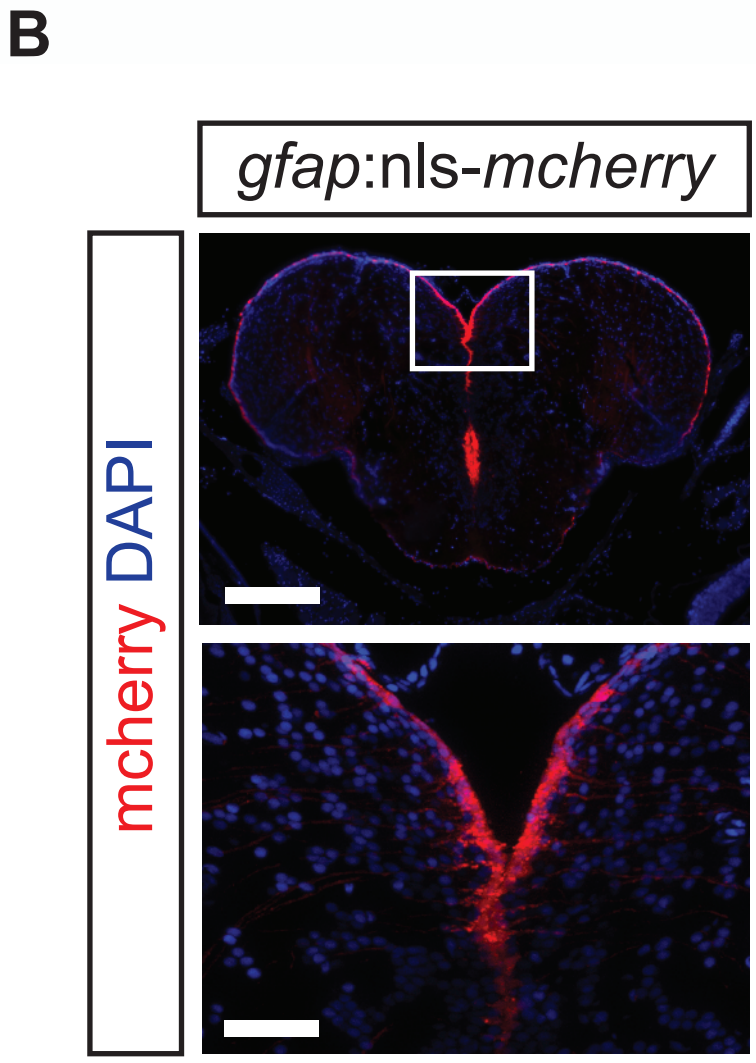
B
gfap:nls-mcherry
mcherry DAPI

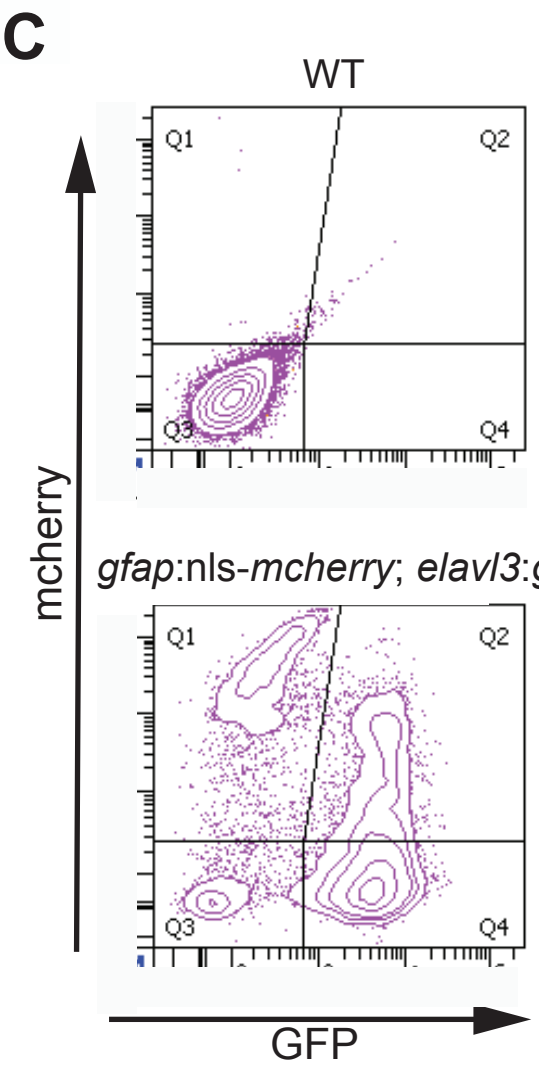
C
WT
Q1
Q2
Q3
Q4
gfap:nls-mcherry; elavl3:gfp
mcherry
GFP

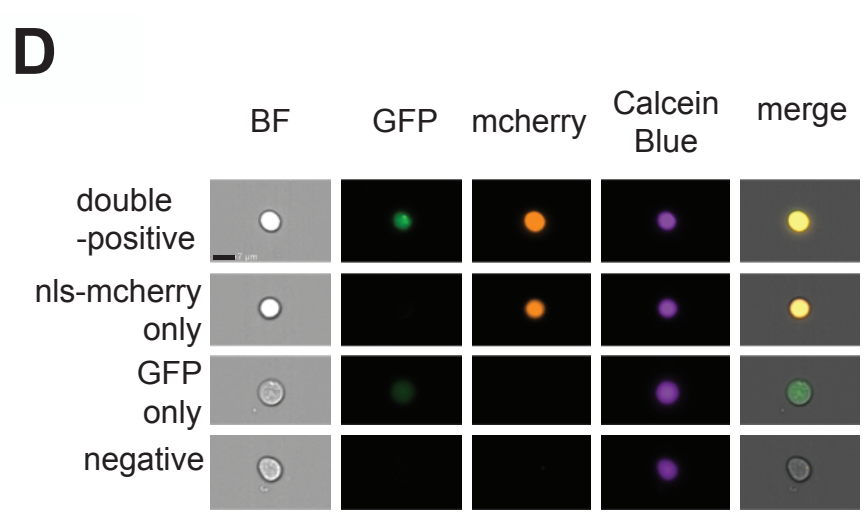
D
BF
GFP
mcherry
Calcein Blue
merge
double -positive
nls-mcherry only
GFP only
negative

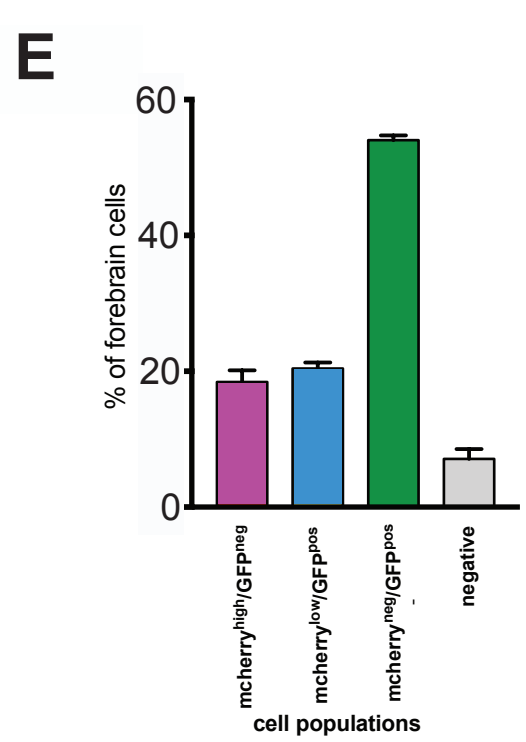
E
% of forebrain cells
60
40
20
0
mcherry^high/GFP^neg
mcherry^low/GFP^pos
mcherry^neg/GFP^pos
negative
cell populations

Figure S1

Figure S1

(A) Representative FACS-plots showing forebrain cells from WT (left) or single transgenic *her4.1*:*mcherry* (middle) and *elavl3:gfp* reporter fish (right), analyzed for mcherry- (y-axis) and GFP-fluorescence (x-axis). (B) Optical section of immunostaining for mcherry in *gfap*:nls-*mcherry* reporter fish, showing expression of the mcherry reporter in RG. Nuclei are stained with DAPI.The lower image shows a magnification of the boxed area of the top panel (C) Representative FACS-plots showing forebrain cells from WT (top) and *gfap*:nls-*mcherry*;*elavl3:gfp* double reporter fish (bottom). Note the clearly separated populations of $mcherry^{high}/GFP^{neg}$, $mcherry^{low}/GFP^{pos}$ and $mcherry^{neg}/GFP^{pos}$ cells. (D) Representative single cells imaged in flow cytometry for $mcherry^{pos}/GFP^{pos}$ (top), $mcherry^{pos}/GFP^{neg}$ (middle, top), $mcherry^{neg}/GFP^{pos}$ (middle,bottom) and , $mcherry^{neg}/GFP^{neg}$ (bottom). At least 20 cells were analyzed and no doublets were seen, excluding that double-positive cells represent doublets. (E) Quantification of cells in the 4 quadrants shown in (B) indicating that $mcherry^{low}/GFP^{pos}$ NBNs can be found in a frequency comparable to $mcherry^{high}/GFP^{neg}$ RGs. N=3; data are presented as mean±SEM. Scale bar = 200μm (B,top), 30μm (B,bottom) or 7 μm (D).

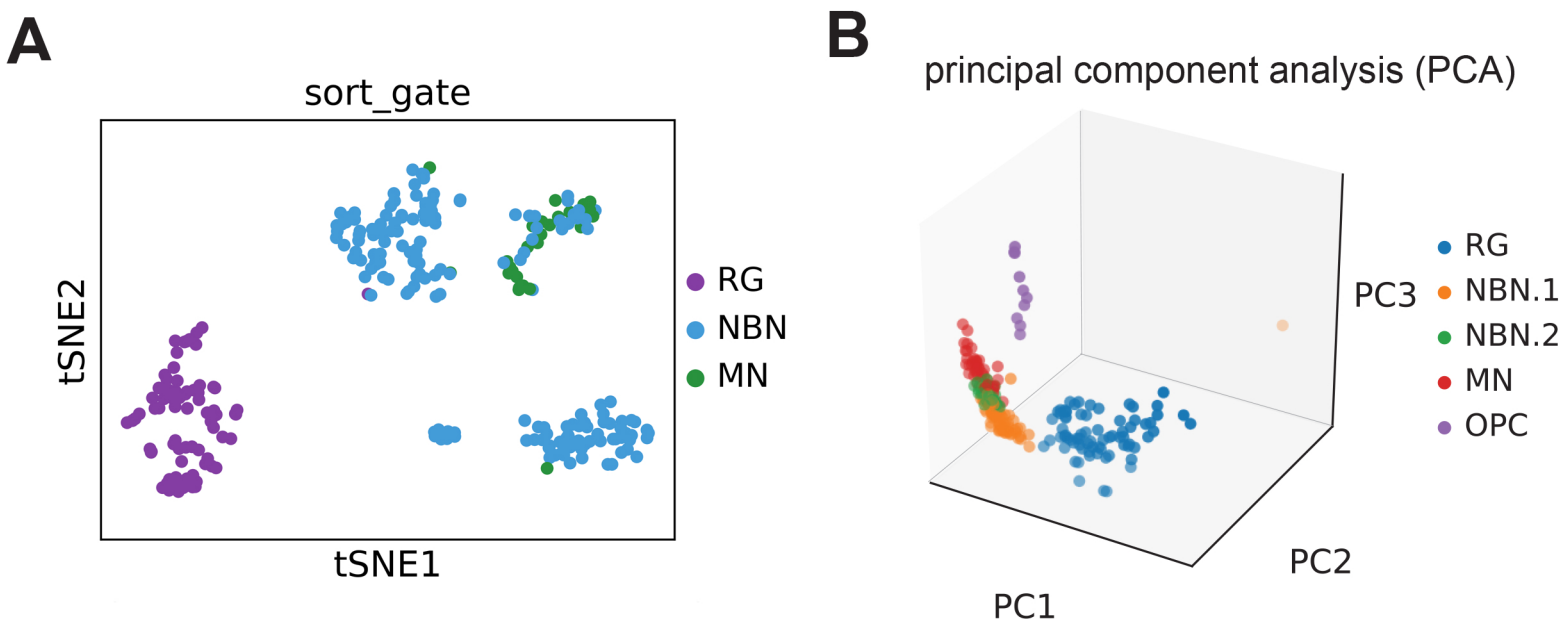

Figure S2

Figure S2

(A) tSNE plot showing the distribution of sorted cell types according to FACS gates (RG (purple), NBNs (cyan), MNs (green)) within the 5 transcriptome-based clusters shown in Figure 2B. The data indicate that RG and MNs each contribute to only one cluster, while NBN are heterogeneous and a subset also forms a common cluster with MNs (B) Plot for dimensionality reduction using principal component analysis (PCA), resulting in similar cluster as those generated with tSNE.

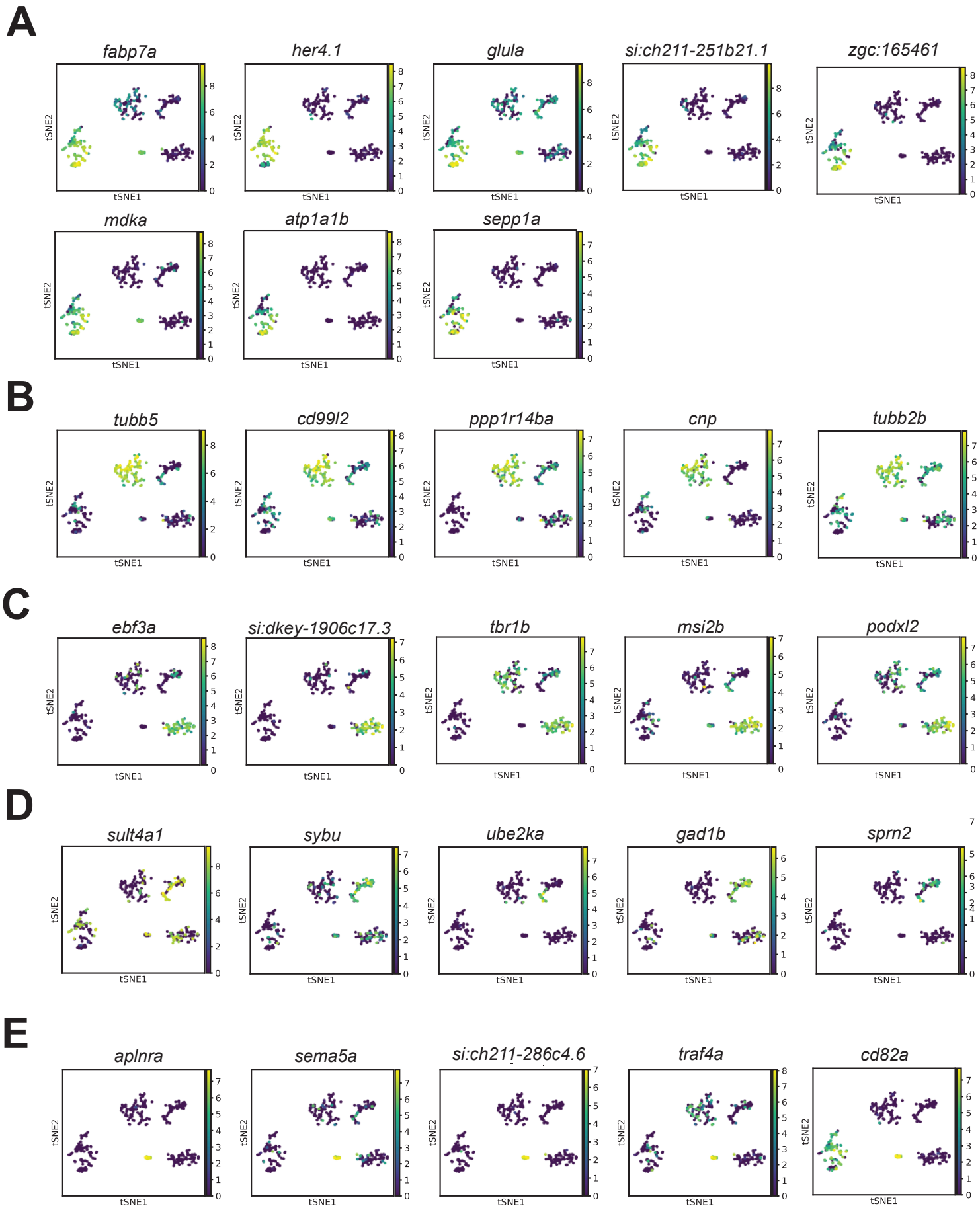

Figure S3

Figure S3

(A) Expression of RG marker genes (*fabp7a*, *her4.1*, *glula*, *si:ch211-251b21.1*, *zgc:165461*, *atp1a1b*, *sepp1a*, *mdka*) in t-SNE plots. Each t-SNE plot consists of n=264 cells. Cells in each plot are colored by their expression of each marker gene according to the adjacent scale. (B) Expression of NBN.1 marker genes (*tubb5*, *cd99l2*, *cnp, ppp1r14ba, tuba2a*) in t-SNE plots as in (A). (C) Expression of NBN.2 marker genes (*ebf3a*, *si:dkey-106c17.3*, *tbr1b*, *msi2b, podxl2*) in t-SNE plots as in (A). (D) Expression of MN marker genes (*sult4a1, sybu*, ube2ka, *gad1b*, *sprn2*) in t-SNE plots as in (A). (E) Expression of OPC marker genes (*aplnra*, *sema5a, si:ch211-286c4.6, traf4a, cd82a*) in t-SNE plots as in (A).

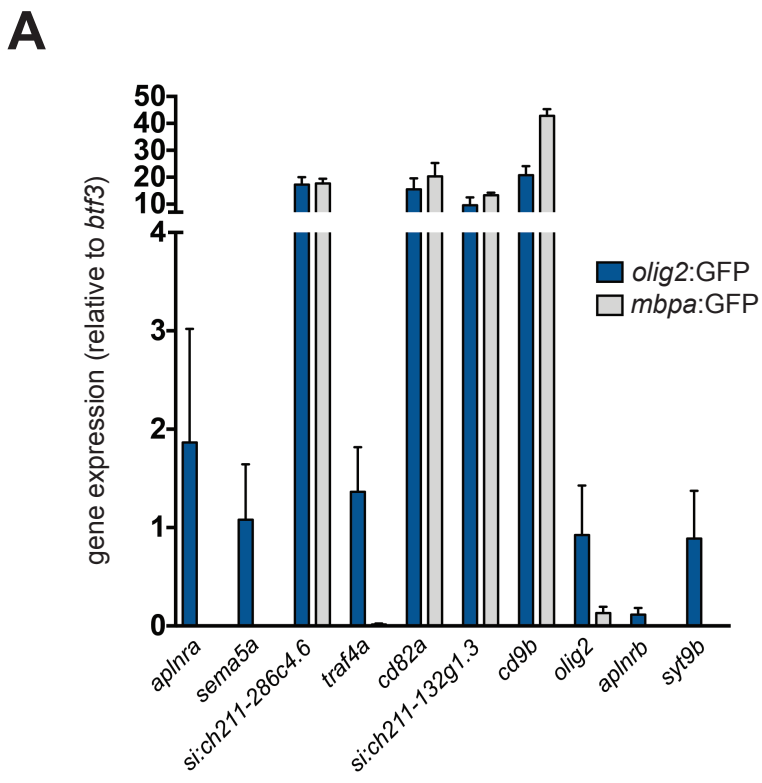

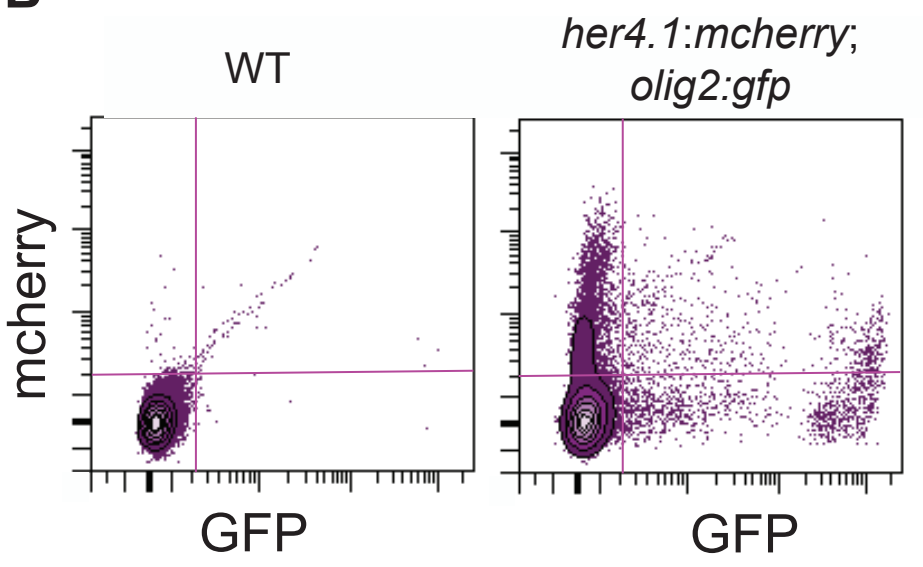

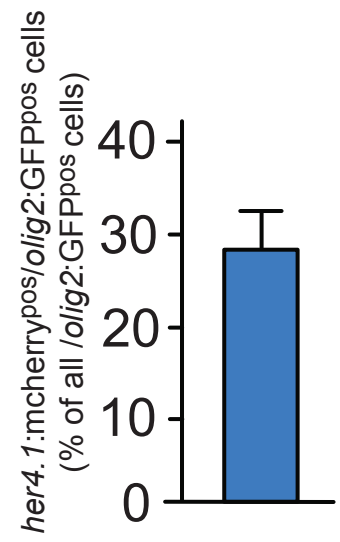

Figure S4

Figure S4

(A) Expression of top 10 OPC marker genes, identified in this study (*aplnra*, *sema5a, si:ch211-286c4.6*, *traf4a*, *cd82a*, *si:ch211132g1.3, cd9b, olig2, aplnrb, syt9b*) in sorted OPCs (*olig2*:GFP^{+}, blue bars) or sorted oligodendrocytes (*mbpa*:GFP+, grey bars) from the adult zebrafish spinal cord. A subset of OPC markers (*aplnra*, *sema5a, traf4a olig2, aplnrb, syt9b*) was specifically expressed in OPC, while *si:ch211-286c4.6, cd82a*, *si:ch211132g1.3 and* cd9b were consistently expressed in the oligodendrocyte lineage. Data are taken from Kroehne et al. (2017). (B) Representative FACS-plots showing forebrain cells from WT (left) or *her4.1*:*mcherry*; *olig2*:*gfp* double-transgenic reporters (right), analyzed for mcherry- (y-axis) and GFP-fluorescence (x-axis). Note the substantial proportion of *her4.1*:mcherry^{pos}/ *olig2*:GFP^{pos} cells. (C) Quantification of *her4.1*:mcherry^{pos}/ *olig2*:GFP^{pos} cells as fraction of all *olig2*:GFP^{pos} cells. N=3; data are presented as mean±SEM.

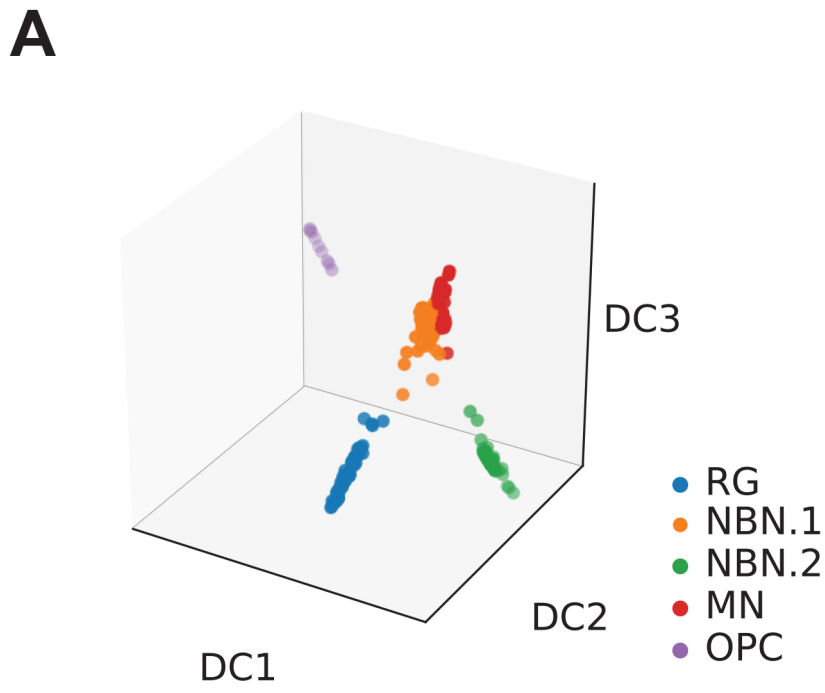

Figure S5

Figure S5

(A) Lineage trajectory analysis of single-cell RNAseq data from RG, NBNs, MNs and OPCs from the adult zebrafish forebrain as shown in Figure 3A, but including OPCs. Color coding corresponds to the different cell clusters identified in Figure 2B. The OPCs are transcriptionally disconnected from the RG and their neuronal progeny. (B) Venn diagram showing overlapping expression of the top 100 marker genes for NBN.1 cells (middle, orange) with the top 100 marker genes of proliferating RG (pRG,left, blue) or quiescent RG (qRG, right, green). Significant statistical overrepresentation of NBN.1 marker genes is found in pRG (9 co-expressed NBN.1 marker genes), but not in qRG (1 co-expressed NBN.1 marker gene). ***=p<0.0001 (C) Diagram of nearest neighbor distance for RG (blue), NBN.1 cells (orange), NBN.2 cells (green), MNs (red) and OPCs (purple) to their most similar mammalian cells from Hochgerner et al. (2018). Each dot represents one cell. A dashed line indicates the cut-off for the 66 percent quantile. Cells within the 66 percent quantile were included into the analysis of corresponding murine cell type heterogeneity (Fig. 4C,D).

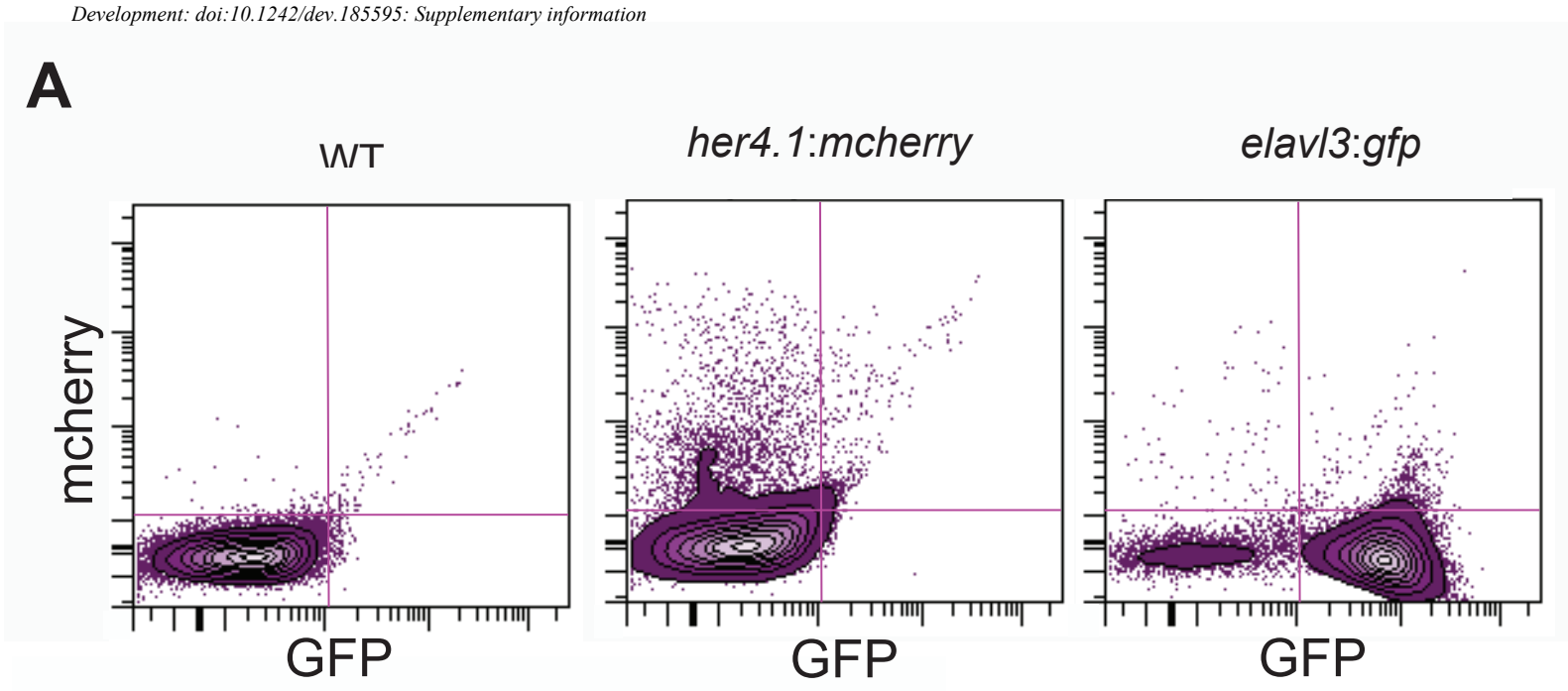
A
WT
her4.1:mcherry
elavl3:gfp
mcherry
GFP
GFP
GFP

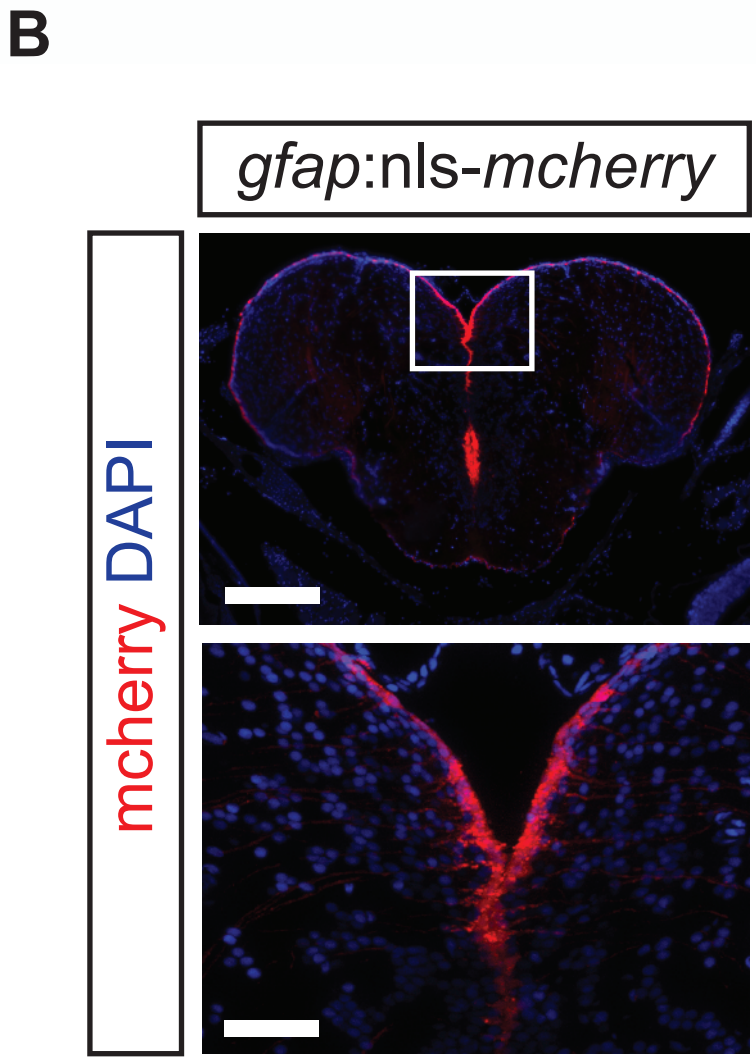
B
gfap:nls-mcherry
mcherry DAPI

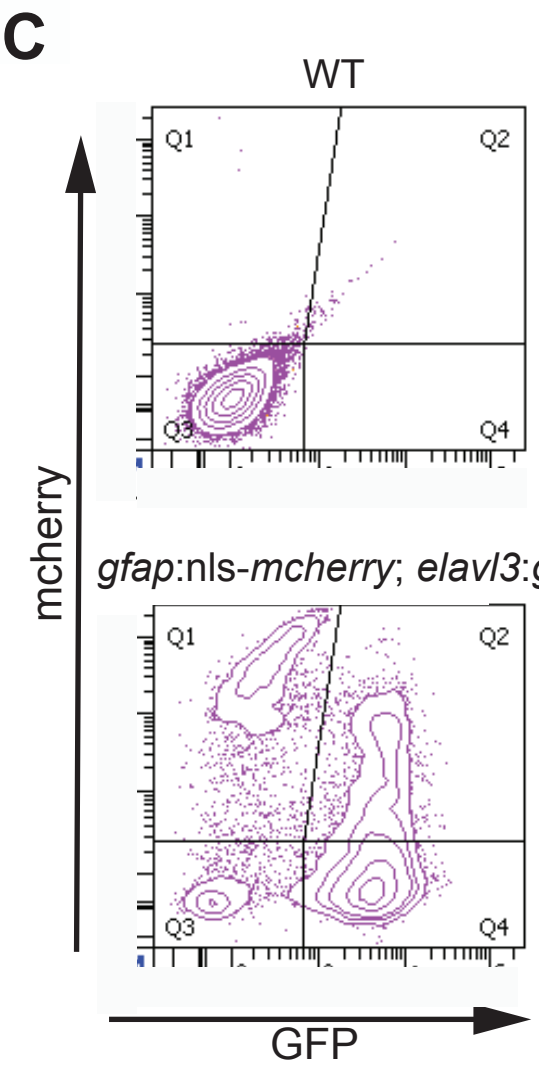
C
WT
Q1
Q2
Q3
Q4
gfap:nls-mcherry; elavl3:gfp
mcherry
GFP

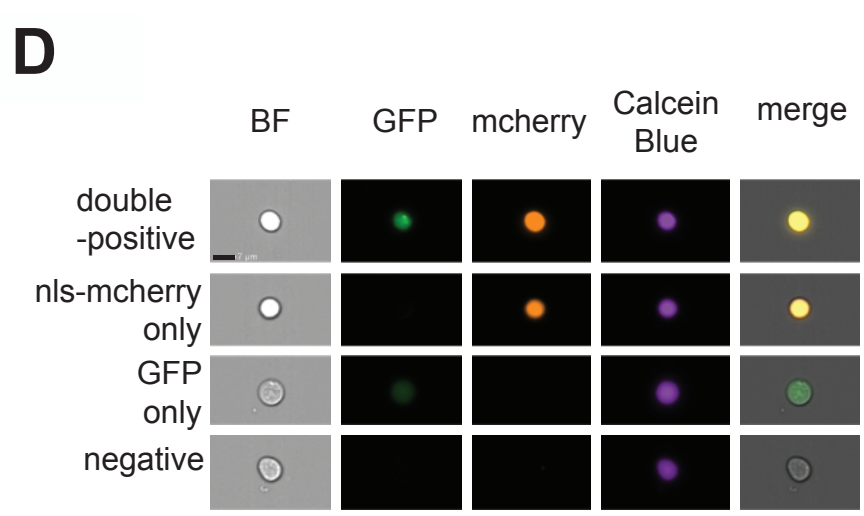
D
BF
GFP
mcherry
Calcein Blue
merge
double -positive
nls-mcherry only
GFP only
negative

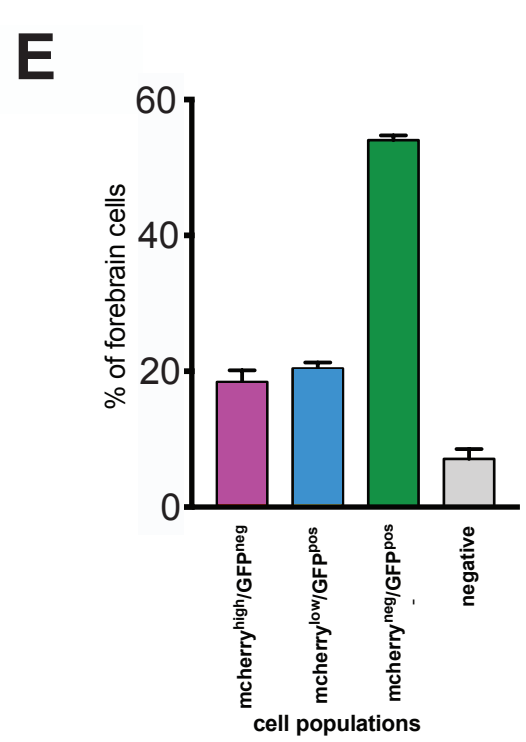
E
% of forebrain cells
60
40
20
0
mcherry^high/GFP^neg
mcherry^low/GFP^pos
mcherry^neg/GFP^pos
negative
cell populations

Figure S1

Figure S1

(A) Representative FACS-plots showing forebrain cells from WT (left) or single transgenic *her4.1*:*mcherry* (middle) and *elavl3:gfp* reporter fish (right), analyzed for mcherry- (y-axis) and GFP-fluorescence (x-axis). (B) Optical section of immunostaining for mcherry in *gfap*:nls-*mcherry* reporter fish, showing expression of the mcherry reporter in RG. Nuclei are stained with DAPI.The lower image shows a magnification of the boxed area of the top panel (C) Representative FACS-plots showing forebrain cells from WT (top) and *gfap*:nls-*mcherry*;*elavl3:gfp* double reporter fish (bottom). Note the clearly separated populations of $mcherry^{high}/GFP^{neg}$, $mcherry^{low}/GFP^{pos}$ and $mcherry^{neg}/GFP^{pos}$ cells. (D) Representative single cells imaged in flow cytometry for $mcherry^{pos}/GFP^{pos}$ (top), $mcherry^{pos}/GFP^{neg}$ (middle, top), $mcherry^{neg}/GFP^{pos}$ (middle,bottom) and , $mcherry^{neg}/GFP^{neg}$ (bottom). At least 20 cells were analyzed and no doublets were seen, excluding that double-positive cells represent doublets. (E) Quantification of cells in the 4 quadrants shown in (B) indicating that $mcherry^{low}/GFP^{pos}$ NBNs can be found in a frequency comparable to $mcherry^{high}/GFP^{neg}$ RGs. N=3; data are presented as mean±SEM. Scale bar = 200μm (B,top), 30μm (B,bottom) or 7 μm (D).

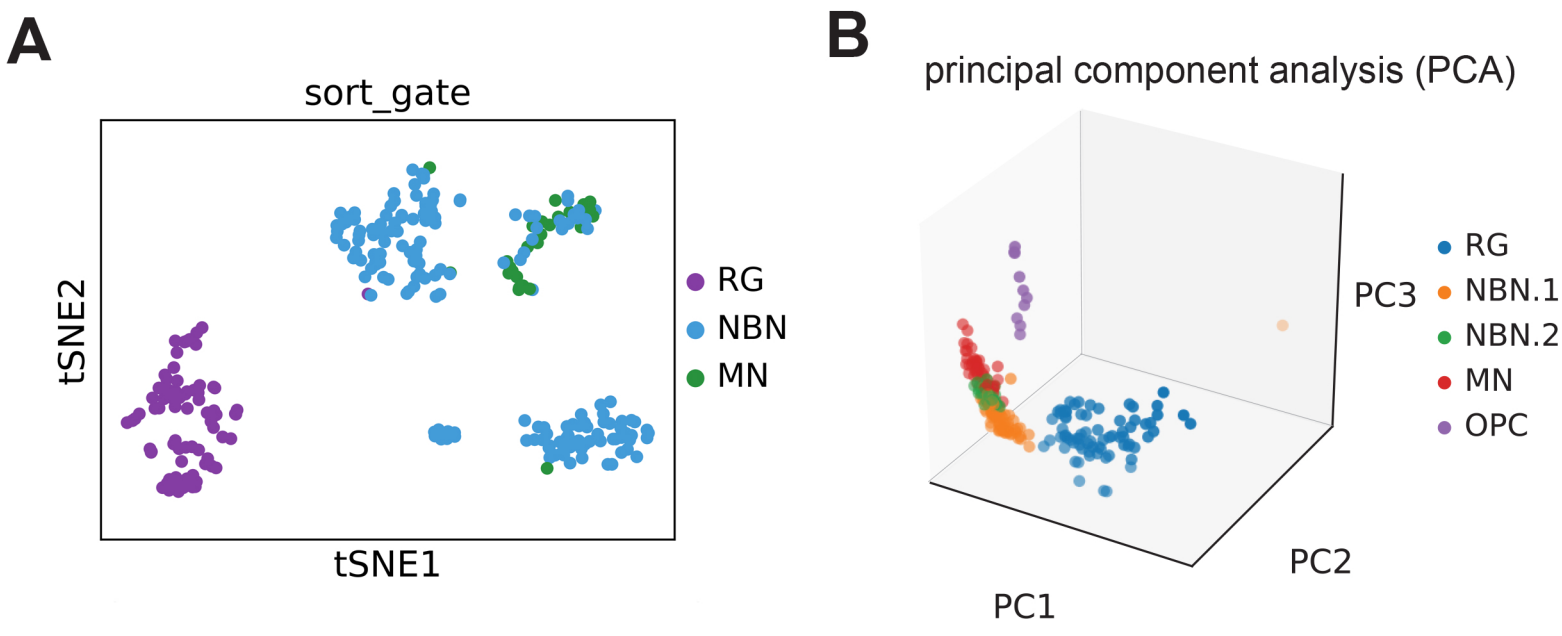

Figure S2

Figure S2

(A) tSNE plot showing the distribution of sorted cell types according to FACS gates (RG (purple), NBNs (cyan), MNs (green)) within the 5 transcriptome-based clusters shown in Figure 2B. The data indicate that RG and MNs each contribute to only one cluster, while NBN are heterogeneous and a subset also forms a common cluster with MNs (B) Plot for dimensionality reduction using principal component analysis (PCA), resulting in similar cluster as those generated with tSNE.

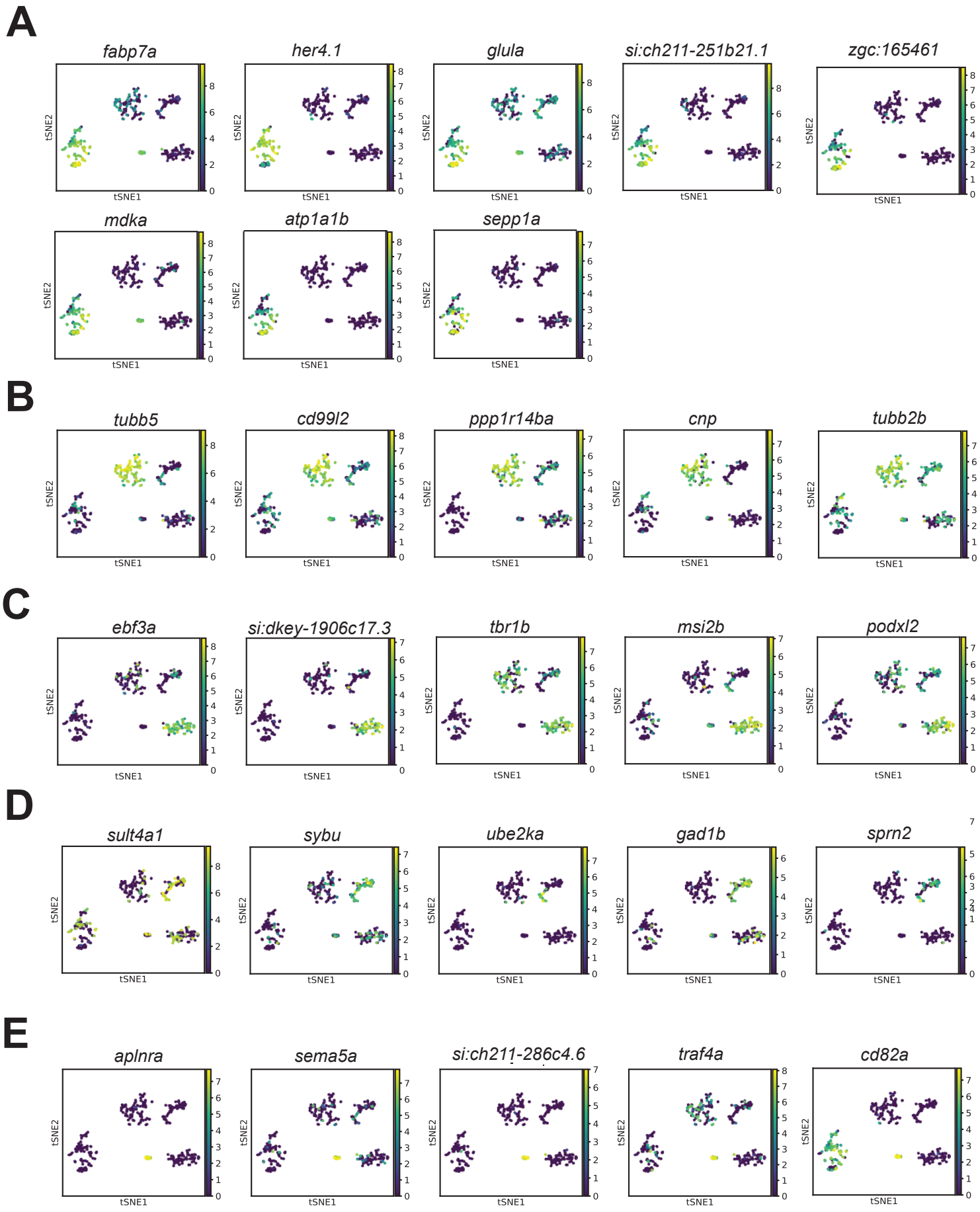

Figure S3

Figure S3

(A) Expression of RG marker genes (*fabp7a*, *her4.1*, *glula*, *si:ch211-251b21.1*, *zgc:165461*, *atp1a1b*, *sepp1a*, *mdka*) in t-SNE plots. Each t-SNE plot consists of n=264 cells. Cells in each plot are colored by their expression of each marker gene according to the adjacent scale. (B) Expression of NBN.1 marker genes (*tubb5*, *cd99l2*, *cnp, ppp1r14ba, tuba2a*) in t-SNE plots as in (A). (C) Expression of NBN.2 marker genes (*ebf3a*, *si:dkey-106c17.3*, *tbr1b*, *msi2b, podxl2*) in t-SNE plots as in (A). (D) Expression of MN marker genes (*sult4a1, sybu*, ube2ka, *gad1b*, *sprn2*) in t-SNE plots as in (A). (E) Expression of OPC marker genes (*aplnra*, *sema5a, si:ch211-286c4.6, traf4a, cd82a*) in t-SNE plots as in (A).

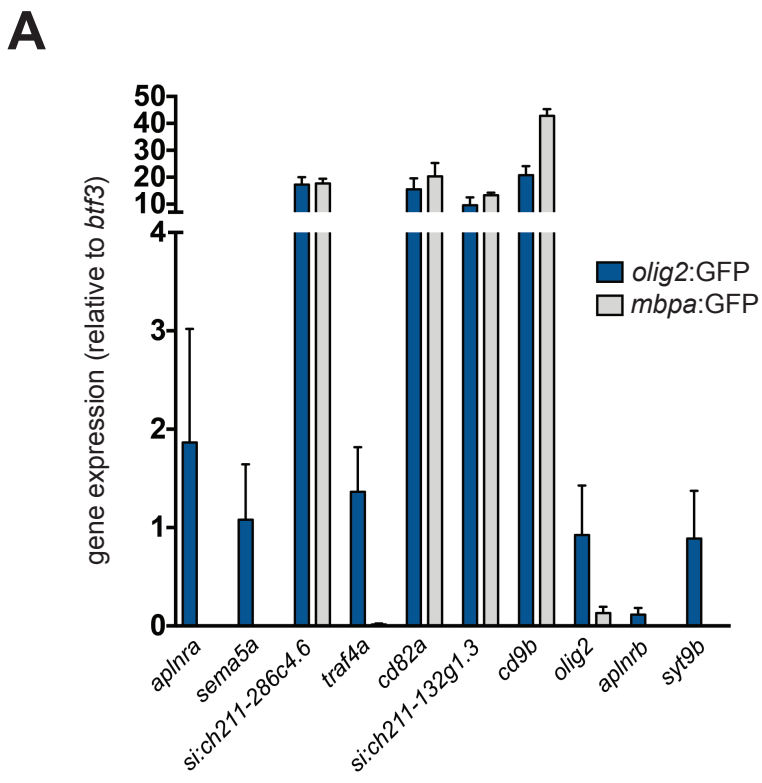

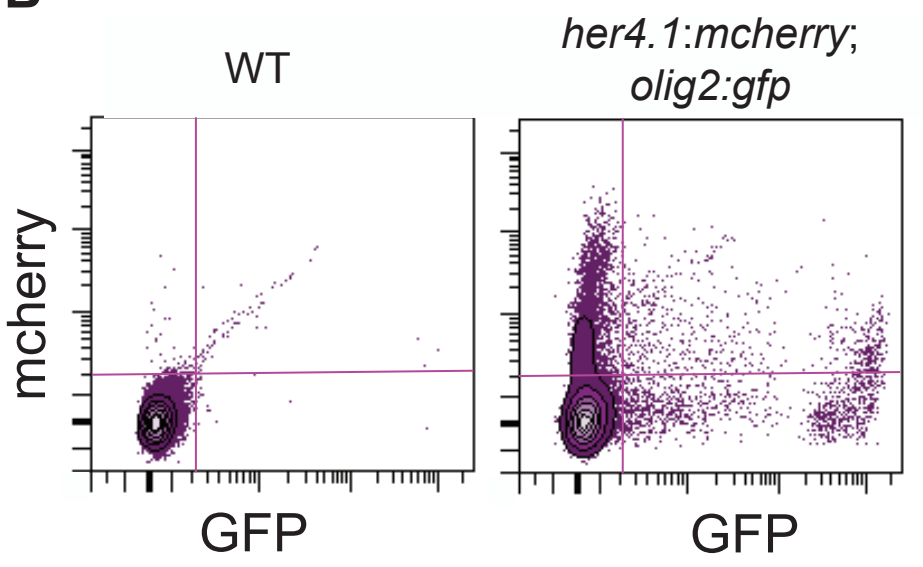

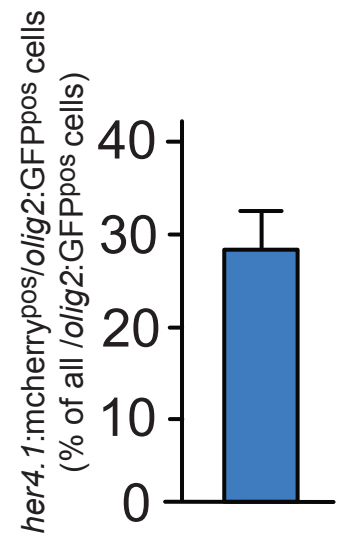

Figure S4

Figure S4

(A) Expression of top 10 OPC marker genes, identified in this study (*aplnra*, *sema5a, si:ch211-286c4.6*, *traf4a*, *cd82a*, *si:ch211132g1.3, cd9b, olig2, aplnrb, syt9b*) in sorted OPCs (*olig2*:GFP^{+}, blue bars) or sorted oligodendrocytes (*mbpa*:GFP+, grey bars) from the adult zebrafish spinal cord. A subset of OPC markers (*aplnra*, *sema5a, traf4a olig2, aplnrb, syt9b*) was specifically expressed in OPC, while *si:ch211-286c4.6, cd82a*, *si:ch211132g1.3 and* cd9b were consistently expressed in the oligodendrocyte lineage. Data are taken from Kroehne et al. (2017). (B) Representative FACS-plots showing forebrain cells from WT (left) or *her4.1*:*mcherry*; *olig2*:*gfp* double-transgenic reporters (right), analyzed for mcherry- (y-axis) and GFP-fluorescence (x-axis). Note the substantial proportion of *her4.1*:mcherry^{pos}/ *olig2*:GFP^{pos} cells. (C) Quantification of *her4.1*:mcherry^{pos}/ *olig2*:GFP^{pos} cells as fraction of all *olig2*:GFP^{pos} cells. N=3; data are presented as mean±SEM.

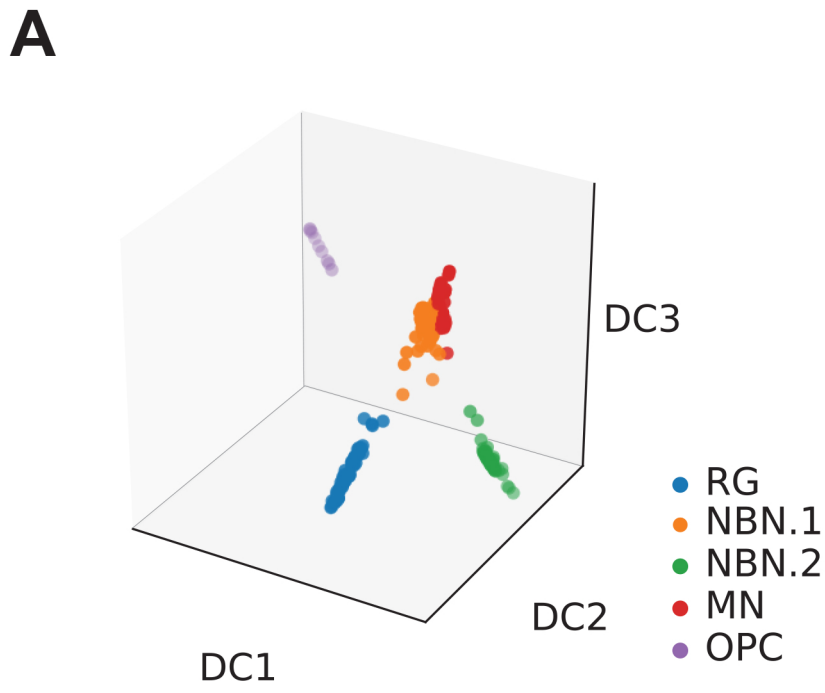

Figure S5

Figure S5

(A) Lineage trajectory analysis of single-cell RNAseq data from RG, NBNs, MNs and OPCs from the adult zebrafish forebrain as shown in Figure 3A, but including OPCs. Color coding corresponds to the different cell clusters identified in Figure 2B. The OPCs are transcriptionally disconnected from the RG and their neuronal progeny. (B) Venn diagram showing overlapping expression of the top 100 marker genes for NBN.1 cells (middle, orange) with the top 100 marker genes of proliferating RG (pRG,left, blue) or quiescent RG (qRG, right, green). Significant statistical overrepresentation of NBN.1 marker genes is found in pRG (9 co-expressed NBN.1 marker genes), but not in qRG (1 co-expressed NBN.1 marker gene). ***=p<0.0001 (C) Diagram of nearest neighbor distance for RG (blue), NBN.1 cells (orange), NBN.2 cells (green), MNs (red) and OPCs (purple) to their most similar mammalian cells from Hochgerner et al. (2018). Each dot represents one cell. A dashed line indicates the cut-off for the 66 percent quantile. Cells within the 66 percent quantile were included into the analysis of corresponding murine cell type heterogeneity (Fig. 4C,D).